Construction and Building Materials 449 (2024) 138480

Contents lists available at ScienceDirect

Construction and Building Materials

journal homepage: www.elsevier.com/locate/conbuildmat

Cyclic flexural performance of seawater sea-sand concrete reinforced with hybrid fibers

Amirhesam Mashayekhi [a], Reza Hassanli [a,*], Yan Zhuge [a], Xing Ma [a], Christopher W.K. Chow [a], Milad Bazli [b], Allan Manalo [c]

[a] Sustainable Infrastructure and Resource Management (SIRM), UniSA STEM, University of South Australia, Mawson Lakes, SA 5095, Australia
[b] Faculty of Science and Technology, Charles Darwin University, Darwin 0810, Australia
[c] Center for Future Materials, School of Engineering, University of Southern Queensland, QLD 4350, Australia

ARTICLE INFO

Keywords:
Cyclic loading
Seawater
Sea-sand
Hybrid fibers
Energy dissipation
PVA
Flexural strength
Fiber reinforced concrete

ABSTRACT

Fiber-reinforced seawater sea-sand concrete (FR-SWSSC), a sustainable alternative to traditional concrete, requires evaluation of its flexural performance under cyclic loading, critical for coastal and marine structures experiencing repeated loads. This study investigated the effect of fiber hybridization and its potential synergistic effects on the cyclic flexural behavior of FR-SWSSC. Incremental cyclic loading was employed for testing FR-SWSSC specimens in four-point cyclic bending. This investigation employed micro-fibers—polypropylene (PPS), polyvinyl alcohol (PVA), basalt (BF)—and macro-fibers—long polypropylene (PPL) and twisted polypropylene (TPPL)—to explore the synergistic influence of fiber size and type (synthetic and natural) on the cyclic flexural behavior. Hybrid-fiber reinforcements were incorporated in two configurations: micro-fibers only and a combination of micro- and macro-fibers. This approach facilitated the evaluation of size-dependent synergy on cyclic flexural properties. According to the results, micro/macro-fiber hybridization significantly improved performance during large deflection cycles. Hybrid TPPL/PVA exhibited 105 % and 664 % greater energy dissipation compared to mono TPPL and PVA, respectively. Similarly, PPS/PVA hybrids displayed a 79 % and 112 % increase in hysteretic damping ratio, over mono PVA and PPS fibers, respectively and reduced damage index and improved strength degradation at large deflections compared to mono fibers. This improvement was attributed to enhanced bonding strength of TPPL or PPS by the strong chemical bonding strength of PVA fibers, which strengthened the surrounding concrete matrix and allowed for a greater contribution from the hybrid components. This study addresses a knowledge gap and paves the way for improved material development through the utilization of a potential sustainable alternative concrete.

1. Introduction

The reliance of construction industry on conventional concrete presents significant environmental challenges, including high freshwater (FW) consumption, disruption of river ecosystems due to sand extraction, and substantial CO_2 emissions from cement production [1–3]. This is particularly problematic for the development of marine engineering projects, where traditional materials often lead to increased costs and longer construction times due to transportation needs [2,4–6]. Developing sustainable alternatives for concrete is critical considering a projected global water crisis [7]. Previous studies have investigated the potential of using eco-friendly materials such as recycled aggregate and supplementary cementitious materials, including slag and fly ash, and their effectiveness in producing more sustainable concrete [8–11]. Seawater sea-sand concrete (SWSSC) emerges as a promising solution for sustainable construction in coastal regions, capitalizing on the readily available seawater (SW) and sea-sand (SS) resources [2,4,6,12–14]. This innovative material offers a multifaceted approach by promoting freshwater conservation, protecting ecological environments, reducing transportation and material costs, as well as lowering carbon emissions in coastal areas, making it a local, cost-effective, and environmentally friendly solution [15].

Concrete structures face substantial durability challenges in marine environments. In terms of durability, incorporating SW and SS into concrete significantly decreased water absorption, sorptivity, and porosity compared to traditional concrete [16–19]. However, this

* Corresponding author.
E-mail address: reza.hassanli@unisa.edu.au (R. Hassanli).

https://doi.org/10.1016/j.conbuildmat.2024.138480
Received 8 August 2024; Received in revised form 20 September 2024; Accepted 22 September 2024
Available online 1 October 2024

inclusion also resulted in increased autogenous and drying shrinkage [17,20,21]. Additionally, in the aggressive environment of SWSSC, due to the presence of various ions [18,21], including sodium (Na^{+}), potassium (K^{+}), chloride (Cl^{-}), sulphate (SO_4^{2-}), calcium (Ca^{2+}), and magnesium (Mg^{2+}), crack control is paramount for the long-term performance and structural integrity of concrete structures [16,22–24]. While fiber-reinforced polymer (FRP) bars address steel corrosion concerns compared to traditional reinforced concrete (RC), crack mitigation remains crucial [25]. Cracks facilitate the ingress of aggressive agents like chlorides and sulfates, accelerating concrete degradation. Here, fiber reinforcement plays a vital role by minimizing crack initiation and propagation, thus enhancing the long-term durability of SWSSC structures. Previous research has demonstrated the effectiveness of both natural and synthetic fibers in improving crack resistance and long-term performance of SWSSC. The addition of polypropylene (PP) fiber to SWSSC reduced water absorption and sorptivity, enhancing its durability [16]. However, steel fibers commonly used in conventional concrete are not suitable for SWSSC due to corrosion susceptibility in the presence of high ion concentrations [26]. Among synthetic fibers, polyvinyl alcohol (PVA) and PP fibers are popular choices due to their affordability, positive influence on concrete properties and environmental resilience [16,22,25–29]. Moreover, the investigation into the durability of polymeric fibers revealed that Polyethylene Terephthalate (PET) fibers exhibit low stability in highly alkaline environments, leading to a rapid decline in fiber strength within concrete matrices [30,31]. The degradation of PET fibers in such conditions significantly increases their instability when embedded in a Portland cement matrix [32,33]. The harsh environment of SWSSC, along with its high chemical reactivity, can potentially impact the performance of fibers and their influence on the long-term behavior of SWSSC, which requires further investigation.

In addition to durability parameters, investigations into the effect of mono-fibers on the strength performance of SWSSC showed a positive impact. The inclusion of fibers, depending on their length, distribution, and bonding strength, can significantly improve the mechanical properties and fracture toughness of SWSSC [16,25,27,34]. While mono-fibers offer benefits, hybrid fiber-reinforced concrete (HFRC) has the potential to overcome the limitations of mono-fibers-length, tensile strength, and bonding strength- by combining micro and macro fibers with specific properties. This can lead to enhanced overall mechanical performance, ductility, toughness, and energy absorption of concrete [25,26,29,35–45]. The influence of fiber geometry, specifically shape and dimension, on the mechanical properties of HFRC is well documented [46,47]. Research suggests that the macroscopic improvement in the mechanical properties of concrete, due to fiber reinforcement stems from the fiber bridging-peeling-slip failure mechanism [46,48]. However, studies have also shown that smooth, short, and straight fibers are readily pulled out during concrete's tensile loading, compromising their effectiveness [49]. Hsie et al. [50] found that combining monofilament and short polypropylene (PP) fibers enhanced the compressive strength, crack resistance, and bending behavior of concrete compared to using single-fiber reinforcement. The short PP fibers effectively dispersed, controlling early crack growth, while the coarser fibers contributed to stiffness and strength. At sufficient quantities, coarse fibers exhibited behavior similar to steel fibers (SF) [50]. An investigation into the influence of hybrid basalt fiber (BF) and PP fiber on the mechanical performance of concrete revealed both positive and negative synergistic effects. The optimal combination, observed at a BF content of 0.15 % and PP fiber content of 0.033 %, resulted in enhancements of 14.1 %, 22.8 %, and 48.6 % in compressive strength, flexural strength, and splitting tensile strength, respectively [51]. The combination of BF/PVA exhibited a significant synergistic improvement in concrete performance. The optimal combination of fibers was found to be 0.1 % PVA and 0.3 % BF, resulting in enhanced compressive strength that were 24.6 % and 8.54 % greater than those of mono PVA and BF, respectively, at the same content [52]. Synergistic effects were observed for the combinations of 0.75 % BF/0.25 %PP and 0.5 % BF/0.5 % glass fiber (GF) and demonstrated the highest mechanical properties improvement over mono PP and BF fibers [53].

There are limited studies on the effect of fiber hybridization on the mechanical performance of SWSSC. Incorporation of hybrid PVA/BF resulted in a significant improvement in the total energy absorption by 44 % and residual compressive strength by 181 % in SWSSC compared to the incorporation of mono BF [25]. The incorporation of hybrid micro/macro fibers SWSSC demonstrated synergistic effects, where the combination of micro- and macro-BF fiber hybridization yielded the greatest synergistic improvement. Notably, the inclusion of micro-fibers primarily contributed to an increase in the first-cracking strength, whereas macro-fibers served to enhance the post-cracking behavior of the composite [26]. The synergistic effects from fiber hybridization significantly enhanced the fracture toughness of SWSSC, with PP fibers combined with BF or PVA fibers resulting in 176 % and 290 % increases in fracture energy, respectively [54]. A review of the literature reveals that previous studies have primarily focused on the influence of mono- and hybrid-fibers on the overall performance of SWSSC under monotonic loading conditions.

Unlike monotonic loading to evaluate the mechanical characteristic of concrete, cyclic loading replicates real-world stresses like wind and traffic, or earthquakes, which are inevitable for the RC structures during the service life [55]. Furthermore, a critical factor influencing the seismic performance of RC structures is their ductility and their ability to dissipate the accumulated seismic energy [56]. Research by Park and Paulay [57] demonstrated that controlled crack formation is essential for this energy dissipation process. This highlights the importance of fibers in concrete and the need to evaluate their effect on the overall performance of concrete under cyclic loading. Previous study indicated that hooked-end steel and macro-polypropylene hybrid fiber can effectively mitigate the stiffness degradation process under cyclic compressive loading [58]. The cyclic tensile behavior of concrete was investigated by incorporating hybrid steel-polypropylene fibers. The results demonstrated that the synergistic effect of SF and PP enhanced the overall tensile properties across multiple levels [59]. The cyclic compressive stress–strain behavior of hybrid SF/PP fibers showed that, with confinement, hybrid fibers significantly enhance concrete's mechanical properties, shifting the failure mode from tensile to shear [60]. Additionally, as the number of cycles increased, both plastic strain energy and hysteretic energy consumption increased. During early cyclic loading, the HFRC primarily retained elastic strain energy with minimal hysteretic energy consumption [61]. The incorporation of SF resulted in 242 % increase in cyclic flexural strength compared to plain concrete [56]. Adding short PP fibers improved the ductility of concrete after peak stress under cyclic compressive loading. It also increased the compressive strength, peak strain, and residual stress of the concrete. However, the effects on elastic modulus and plastic strain were not significant [62].

FR-SWSSC presents a promising and sustainable alternative for coastal construction. However, a comprehensive understanding of its flexural behavior under cyclic loading is crucial for ensuring the safety, serviceability, and efficiency of these structures. Marine environments subject structures to a combination of waves, tides, and seismic events, all of which induce cyclic loading. Previous research suggests that fiber incorporation improves the ductility, energy dissipation, and crack control of concrete under cyclic loads [56,63,64]. Utilizing the synergistic effects of hybrid fibers, where combined properties surpass those of individual fibers, researchers can establish reliable design parameters for engineers, ultimately promoting sustainable and efficient coastal construction. Notably, existing research primarily focuses on either the static flexural behavior of FR-SWSSC [16,27] or the cyclic response of conventional concrete with hybrid fibers [63,65,66]. Moreover, the unique chemical reactivity of SWSSC has the potential to influence interfacial bonding and fiber synergy, both of which are critical factors in hybrid fiber performance. This study aims to bridge this knowledge gap by investigating the specific interaction between SWSSC and hybrid fibers under cyclic loading and evaluating the flexural performance of FR-SWSSC. This study comprehensively investigates the effect of hybrid fibers, combining micro and macro fibers, on the cyclic flexural response of FR-SWSSC compared to mono-fibers. These findings contribute to sustainable construction practices by paving the way for further research on hybrid FR-SWSSC.

2. Experimental work

2.1. Material properties

This research employed a sustainable approach by incorporating ground granulated blast furnace slag (GGBS) as a partial replacement for ordinary Portland cement (OPC) at a 65:35 ratio, thereby reducing CO_2 emissions [67–69]. Seawater (SW), obtained from Adelaide coast and exhibiting elevated chloride and sulphate concentrations (360 and 76 times higher than tap water, respectively), was carefully stored to prevent contamination prior to utilization. Natural sand (NS) and sea-sand (SS) were employed as fine aggregates for FWNS and SWSSC, respectively, with a maximum particle size of 2.5 mm for NS and 0.5 mm for SS. Scanning electron microscopy (SEM) analysis (Fig. 1) revealed a smooth, rounded morphology for SS particles compared to the rough surface texture of NS. Inductively Coupled Plasma Optical Emission Spectroscopy (ICP-OES) analysis identified higher lead (Pb) and selenium (Se) concentrations in sea-sand compared to natural sand. Specifically, the concentrations of Pb and Se in sea-sand were 1.05 mg/kg and 2.8 mg/kg, respectively, while in natural sand they were 0.084 mg/kg and 0.174 mg/kg, respectively. However, both elements remained below the established landfill hazardous material limits [70]. Crushed basalt from a local quarry served as the coarse aggregate, with a maximum particle size of 14 mm.

The selection of fiber types and dosages was carefully considered to balance performance, cost-efficiency, and environmental impact. For fiber reinforcement, a combination of synthetic and natural fibers—including micro-fibers (PPS, PVA, and BF) and macro-fibers (PPL and TPPL)—was employed without surface treatment to maintain cost-efficiency. This selection ensures a diverse range of mechanical properties, including tensile strength and stiffness, that align with the objective of enhancing SWSSC performance. Basalt fibers were implemented for their high tensile strength, cost-effectiveness, and environmental benefits. Details and characteristics of these fibers are presented in Table 1. Macro-fibers with similar lengths but varying aspect ratios and stiffness were included to analyse their impact. An eco-friendly macro-fiber composed of recycled plastic (PPL) and commercially available in Australia (eMesh by FIBERCON) was incorporated to align with the aim of promoting sustainability in construction practices. Consistent micro-fiber length was maintained to ensure minimal influence on the results, while a range of micro-fibers with varying tensile strengths, Young's modulus, and aspect ratios were utilized.

2.2. Mix proportions and test specimens

Twenty-three concrete mixes were produced, aiming for a compressive strength of 25 MPa. Details of the mix proportions are provided in Table 2. To ensure a workable fresh concrete mix suitable for structural applications, a slump of 150–200 mm was targeted without the incorporation of superplasticizers. The experiment was divided into four series. Series I comprised plain concrete (FWNS and SWSSC), which served as the control groups. Series II focused on mono-fiber types, each with a dosage of 0.25 %, to explore the effects of different fiber types. Series III utilized combinations of micro-fibers with a total dosage of 0.25 %, investigating the synergistic effects of micro-fibers in the hybrid system and their impact on the performance of SWSSC. Series IV examined the effects of combining micro and macro-fibers, also with a total dosage of 0.25 %. The choice of a 0.25 % fiber dosage was intended to ensure optimal dispersion of fibers throughout the concrete matrix while avoiding workability problems associated with higher fiber contents, as indicated by previous research [16,22,27]. Trials conducted in this study validated that the 0.25 % dosage preserved both workability and suitable fiber distribution, consistent with earlier findings and ensuring the effective performance of the fiber-reinforced concrete. This dosage was considered suitable for practical applications, particularly in scenarios where maintaining a workable concrete mix without superplasticizers is essential. The inclusion of various fiber types and combinations across the series allowed for a detailed investigation of their individual and synergistic effects on the overall performance of SWSSC.

Hybrid fiber mixtures were prepared using two different ratios (33 % and 66 %) for each component. Adjusting the proportions in these hybrid systems allows for an evaluation of how the distinct mechanical properties—such as tensile strength, stiffness, and bonding behavior—of the fibers interact within the concrete matrix, resulting in a synergistic effect on performance. For example, the study investigated two PPL/PVA hybrid combinations, designated 0.33PPL/0.66PVA and 0.66PPL/0.33PVA. The 33 % PPL and 66 % PVA combination highlights the impact of high tensile strength and stiffness of PVA fibers, while still utilizing the sustainability and length benefits of PPL fibers. Conversely, the 66 % PPL and 33 % PVA mixture emphasizes the mechanical properties of PPL, while exploring the advantages of PVA fibers. This approach effectively demonstrates the influence of fiber types in hybrid systems and their impact on the overall performance of SWSSC.

Two 100 mm × 100 mm × 350 mm prism samples were cast for cyclic and monotonic flexural test for each mixture based on AS 1012.11 [71]. Following casting, beam samples were demolded after 24 hours and maintained in a moist curing environment at 23°C ± 2°C for one day

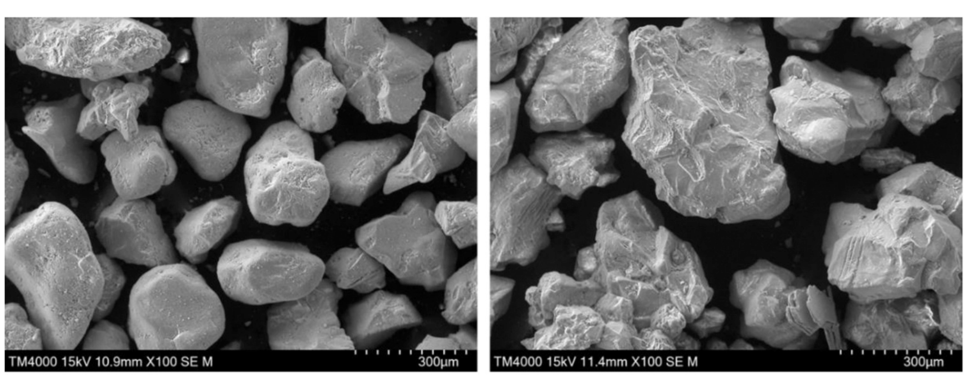

a) Sea-sand b) Natural sand

Fig. 1. SEM analysis of a) sea-sand and b) natural sand.

Table 1
Physical properties of fibers.

Fibers		Specific gravity	Length (mm)	Diameter (μm)	Thickness (μm)	Tensile strength (MPa)	Young's modulus (GPa)	Chemical resistance
Micro	PPS	0.91	6	18	—	600	9.5	Excellent
	PVA	1.3	8	38	—	1600	40	Excellent
	BF	2.8	7	15	—	2900	85	Excellent
Macro	PPL	0.91	47	—	<500	400	6	Excellent
	TPPL	0.91	54	800	—	620	9.5	Excellent

Table 2
Concrete mix design [25].

Groups	Concrete Mix	Water (kg/m^3)		Gravel (kg/m^3)	Binder (kg/m^3)		Sand (kg/m^3)		Fiber (kg/m^3)					28-day f_c (MPa)
		FW	SW		OPC	GGBS	NS	SS	PPS	PVA	BF	PPL	TPPL	
Plain	FWNS	256	256	995	126	234	785	—	—	—	—	—	—	28.5
	SWSS	—	—				—	785	—	—	—	—	—	27.6
Mono	PPS	—	256	995	126	234	—	785	2.28	—	—	—	—	27.2
	PVA								—	3.25	—	—	—	28.9
	BF								—	—	6.63	—	—	27.4
	PPL								—	—	—	2.28	—	28.6
	TPPL								—	—	—	—	2.28	29.0
Hybrid micro	0.33PPS/0.66BF	—	256	995	126	234	—	785	0.76	—	4.41	—	—	27.9
	0.66PPS/0.33BF								1.52	—	2.21	—	—	28.2
	0.66PVA/0.33BF								—	2.17	2.21	—	—	31.1
	0.33PVA/0.66BF								—	1.08	4.41	—	—	27.0
	0.33PPS/0.66PVA								0.76	2.17	—	—	—	27.3
	0.66PPS/0.33PVA								1.52	1.08	—	—	—	26.9
Hybrid macro/micro	0.33PPL/0.66PPS	—	256	995	126	234	—	785	1.52	—	—	0.76	—	27.2
	0.66PPL/0.33PPS								0.76	—	—	1.52	—	26.4
	0.66PPL/0.33PVA								—	1.08	—	1.52	—	31.9
	0.33PPL/0.66PVA								—	2.17	—	0.76	—	31.1
	0.33PPL/0.66BF								—	—	4.41	0.76	—	31.5
	0.66PPL/0.33BF								—	—	2.21	1.52	—	31.5
	0.33TPPL/0.66PVA								—	2.17	—	—	0.76	30.3
	0.66TPPL/0.33PVA								—	1.08	—	—	1.52	30.5
	0.33TPPL/0.66BF								—	—	4.41	—	0.76	28.5
	0.66TPPL/0.33BF								—	—	2.21	—	1.52	29.6

before being transferred to a lime-saturated water bath for 28 days, and then air-cured for 365 days to be tested. The specimens were prepared according to AS 1012.2 [72].

2.3. Cyclic flexural test setup and procedure

The cyclic performance of FR-SWSSC specimens was investigated through four-point cyclic bending following AS 1012.11 [71]. The experimental setup is depicted in Fig. 2. A 100 kN Instron testing machine, capable of displacement and load control, was employed for the flexural testing. The beam specimen was simply supported with a 300 mm span between the supports. To achieve pure bending in the beam, two-point loads spaced 150 mm apart were applied simultaneously. Both load and deflection data were collected automatically by a computer system. The mid-span deflection of the beam specimens was monitored using a linear variable differential transducer (LVDT). The loading procedure consisted of two distinct steps: displacement-controlled and load-controlled. During the loading phase, displacement control was applied at a constant rate of 0.05 mm/min for all plain and FR-SWSSC specimens. This rate was consistent with those used in previous studies on the flexural performance of fiber-reinforced concrete [34,65,73]. Conversely, unloading utilized load control until a near-zero load state was achieved. The specific cyclic loading protocol is illustrated in Fig. 3. This loading protocol effectively incorporates potential real-world experiences of FR-SWSSC structures, which may

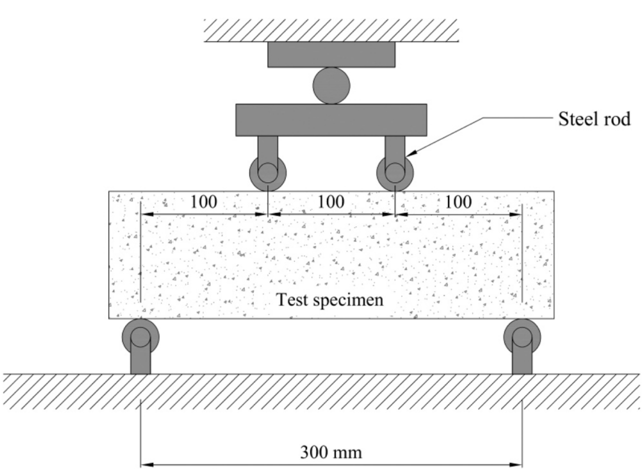

Fig. 2. Cyclic flexural test setup.

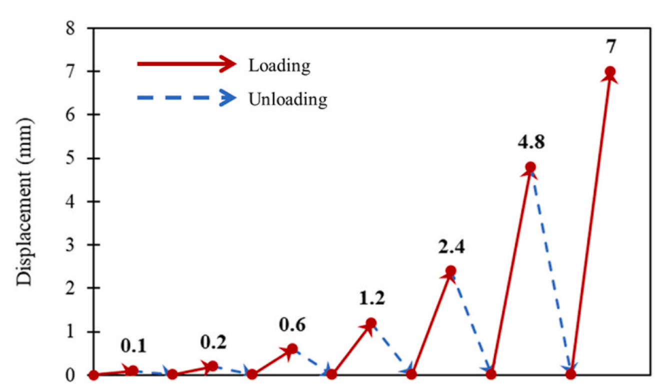

Fig. 3. Cyclic loading protocol.

undergo significant lateral movements due to factors such as seismic events or extreme weather conditions. Additionally, by considering displacement-controlled loading and accommodating higher displacements, the impact of incorporating large fibers can be better investigated.

3. Results and discussions

3.1. Cyclic flexural behavior of FR-SWSSC

3.1.1. Load-mid-span deflection behavior

Figs. 4 and 5 illustrate the load-deflection and backbone curves, respectively, resulting from the cyclic flexural behavior of FR-SWSSC across various concrete mixes. As anticipated, plain SWSSC and FWNS exhibited brittle failure due to a lack of fibers, indicated by a sharp post-peak load drop. Crack initiation and propagation within the concrete at peak point resulted in this behavior. SWSSC displayed marginally higher peak load and superior post-peak performance compared to FWNS, evidenced by a greater residual load capacity during unloading. SEM images in Fig. 6 revealed that SWSSC exhibited a denser structure, consistent with findings from previous studies [22,25,74]. This can be attributed to the higher concentration of portlandite in SWSS, which effectively filled gaps and pores. Moreover, the formation of ettringite was significantly more pronounced in SWSS than in FWNS, likely due to the use of seawater [25,74], further contributing to pore filling and creating a more uniform structure. As shown in Fig. 1, the smoother, more rounded shape of SS compared to NS may enhance its interfacial bond with the cement paste. In contrast, the irregular and angular shape of NS can potentially create more voids and micro-cracks within the matrix, resulting in a weaker bond with the cement paste. The denser matrix resulted in a stronger interfacial bond between the aggregate and cement paste, which ultimately led to the observed improvements in load capacity and post-peak behavior for the SWSSC mixture.

The results demonstrated the effectiveness of mono-fiber inclusion in reducing peak deflection. The incorporation of mono PPS and PVA micro-fibers significantly enhanced peak load capacity. This improvement can be explained by a synergistic mechanism involving fiber bridging, pull-out resistance, and early crack control, where the high tensile strength of PVA and BF fibers played a critical role. Prior research reported chemical bonding of PVA and BF within the concrete matrix. This phenomenon was further substantiated by the SEM analysis depicted in Fig. 7, where both PVA and BF displayed chemical bonding with the SWSSC matrix. Notably, PVA fibers exhibited a greater degree of chemical bonding strength compared to BF. Conversely, PPS fibers demonstrated a weak interfacial bond with concrete matrix. Among the microfibers, PPS exhibited the highest peak strength and the lowest peak deflection. Previous studies have shown that the initial fracture toughness of PPS fibers is higher than that of PVA and BF [34]. This higher fracture toughness, combined with better distribution and a higher quantity (at a 0.25 % dosage), likely contributed to achieving the highest peak strength in this study by providing superior reinforcement before cracking. However, the lower bonding strength and elastic modulus of PPS fibers led to fiber pull-out or breakage after cracking, which limited their bridging effect and inelastic behavior, resulting in lower deflection. The impact of micro-fibers on post-peak response was minimal, likely due to their short length, which limited their ability to bridge macro-cracks after peak stress. In contrast, macro-fibers such as PPL and TPPL significantly improved post-peak behavior in comparison to the plain SWSSC mixture. PPL fibers exhibited substantially higher load capacity at larger deformations, attributed to their superior mechanical bonding facilitated by their length, stiffness, and rough surface. Additionally, micro-fibers, compared to macro-fibers (especially TPPL), showed a greater tendency toward deflection-softening behavior.

The impact of micro-fiber hybridization on SWSSC behavior under cyclic loading was influenced by the fiber type and dosage in the hybrid system. Hybrid micro-fibers reduced peak deflection compared to mono micro-fibers, attributed to an improved elastic modulus achieved through hybridization [25]. Among the micro-fibers studied, BF was the most effective in reducing peak deflection in the hybrid system. The PVA/PPS hybrid increased load-bearing capacity compared to

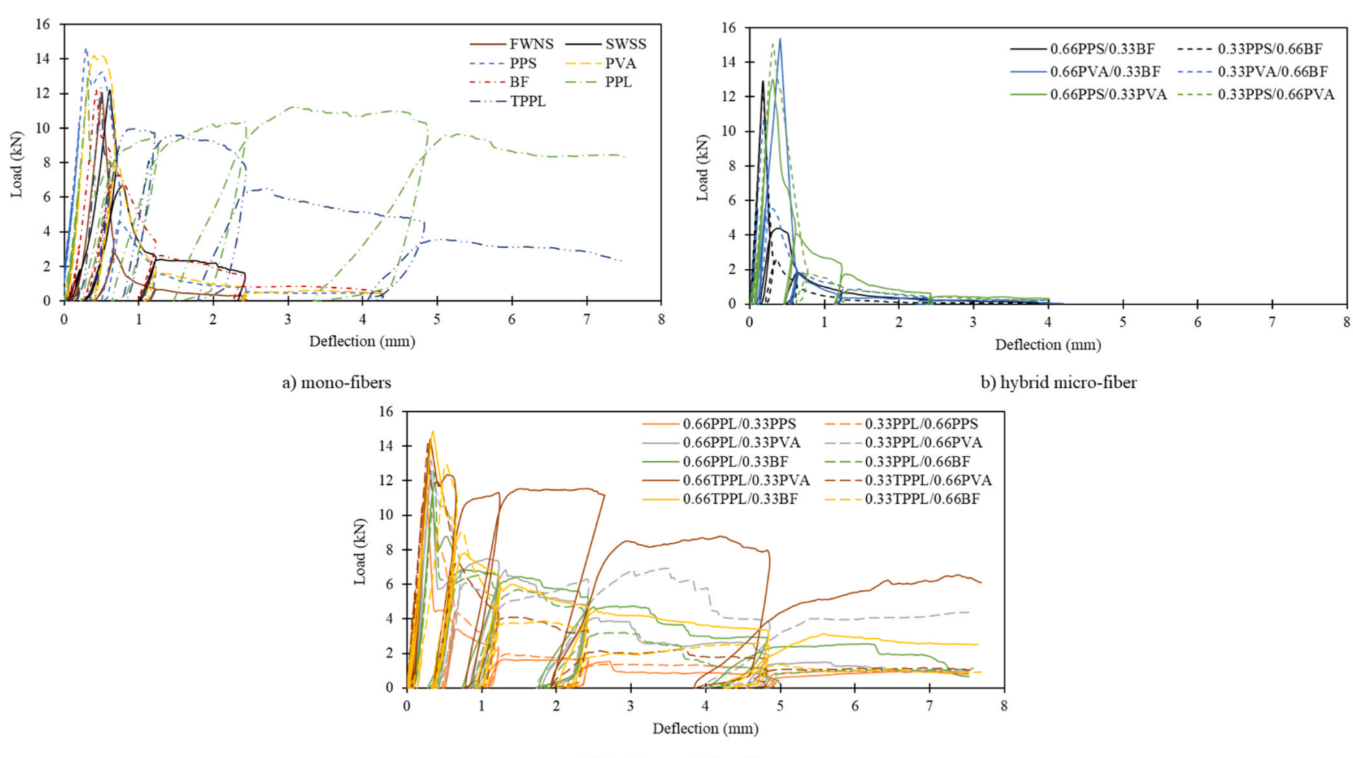

Fig. 4. Load-deflection curves of FR-SWSSC mixtures with different fiber reinforcements, (a) mono-fibers, (b) hybrid micro-fiber, and (c) hybrid macro/micro-fiber.

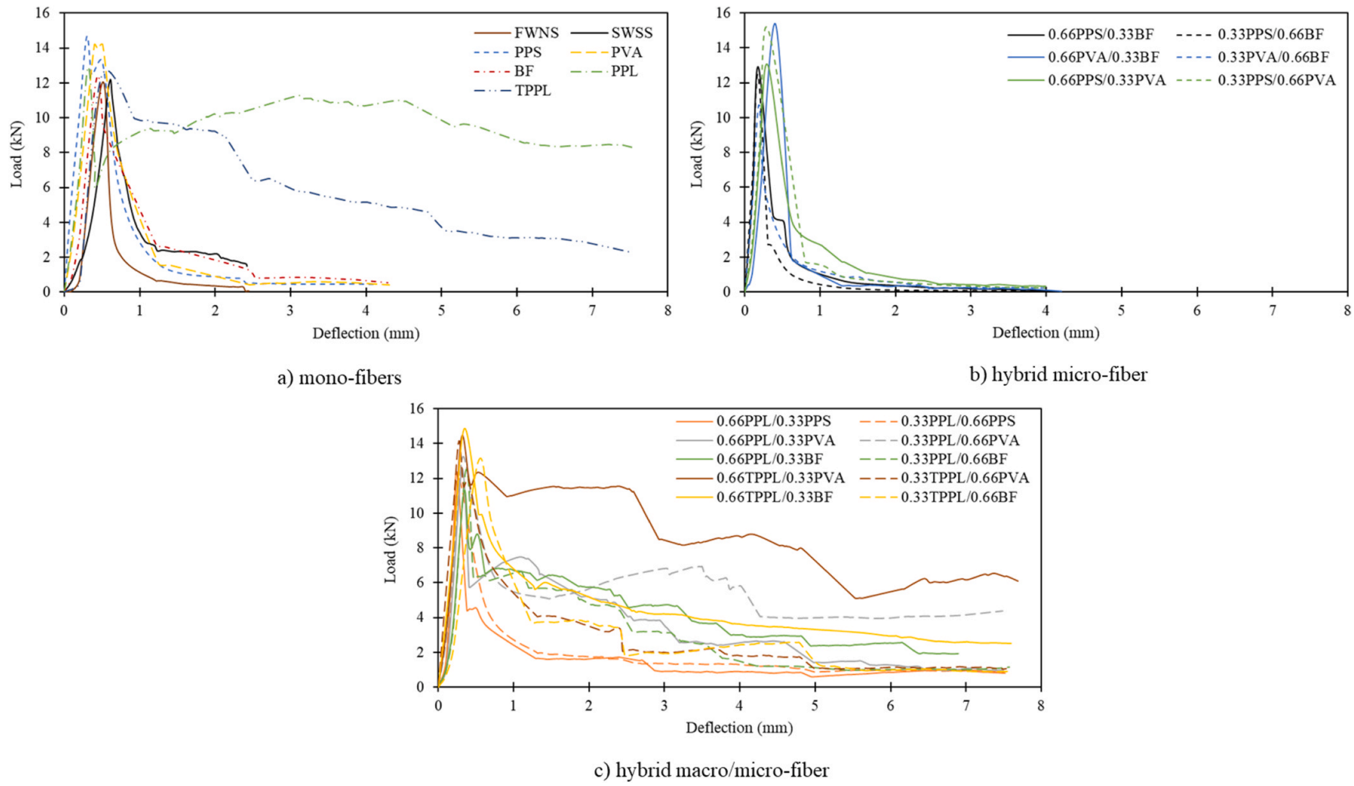

Fig. 5. Backbone curves of load-deflection behavior in FR-SWSSC with different fiber reinforcements: (a) mono-fiber, (b) hybrid micro-fiber, and (c) hybrid macro/micro-fiber.

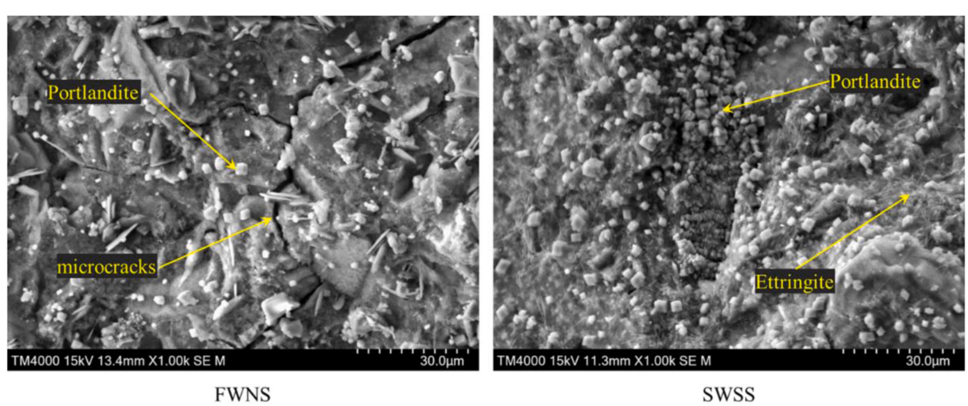

Fig. 6. Microstructure of SWSSC and FWNS using SEM images.

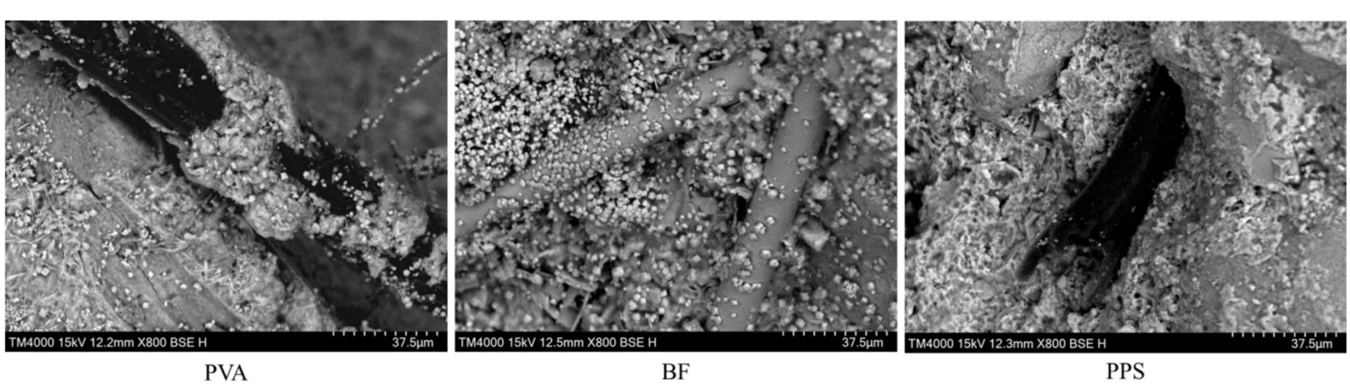

Fig. 7. Microstructure of FR-SWSSC reinforced with micro-fibers using SEM images.

mono-fibers. While peak deflection remained unchanged with PPS/PVA compared to mono PPS, it decreased by 39 % versus mono PVA. Specifically, the 0.33PPS/0.66PVA hybrid significantly enhanced peak strength but decreased post-peak strength across subsequent cycles. This was likely due to a synergistic effect, where PVA enhanced PPS fiber bonding, contributing to a more cracking strength and superior strength attainment. However, after crack initiation and reaching the peak point, the absence of fibers capable of crack control and bridging resulted in a substantial decrease in post-peak load-bearing capacity.

Similar observations were made with PPS/BF hybridization, where partial replacement of BF with PPS resulted in a marginal increase in ultimate strength compared to mono BF but exhibited a weaker post-peak response compared to both mono PPS and BF fibers. Hybridizing PPS/BF resulted in lower peak deflection and a decreased pre-peak slope compared to mono fibers. This effect could be attributed to the enhanced elastic modulus of concrete achieved through hybridization, as reported previously [25]. The PVA/BF combination in the hybrid system was highly sensitive to the fiber ratio. Notably, 0.33PVA/0.66BF significantly reduced peak deflection (by 56 % and 63 % compared to single BF and PVA fibers, respectively), whereas the 0.66PVA/0.33BF ratio had minimal effect. Moreover, the 0.66PVA/0.33BF combination improved peak strength compared to both individual PVA and BF fibers but exhibited a weaker post-peak response and lower strength throughout subsequent cycles. Among all micro-fiber hybridizations, the 0.66PVA/0.33BF combination resulted in the highest peak strength. This behavior could be attributed to the enhanced bonding strength of PVA fibers facilitated by BF fibers, demonstrating the synergistic effect of PVA/BF on bonding strength and elastic modulus, which led to higher strength and improved cracking resistance. However, this combination also increased brittleness, causing a sharp decline in load-bearing capacity beyond the peak point.

Micro/macro fiber hybridization showed that micro-fibers with strong bonding to the concrete matrix (PVA and BF) significantly enhanced the overall bonding strength of macro-fibers in the hybrid system. This improvement resulted from micro-fibers reinforcing the surrounding matrix of macro-fibers, as evidenced by SEM images in Fig. 8. Replacing TPPL fibers with BF increased ultimate strength while reducing peak deflection, and this combination improved post-peak behavior compared to mono BF fibers, which endured more cycles. The 0.66TPPL/0.33BF hybrid exhibited superior strength and post-peak performance over mono TPPL and BF, with increases of 49 % and 58 % in strength, respectively. This was likely due to enhanced bonding strength provided by BF, along with TPPL fiber properties including distribution and flexibility. The TPPL/PVA hybrid outperformed TPPL/BF in post-peak behavior with minimal impact on ultimate strength. Notably, the 0.66TPPL/0.33PVA combination achieved significantly higher strength at elevated cycles compared to both mono PVA and TPPL fibers. A higher TPPL dosage in hybrid systems proved more effective, showing positive synergy where TPPL bridges macro-cracks and PVA or BF enhances bond strength, resulting in superior overall performance.

PPL/PPS hybridization did not significantly differ from mono PPS in cyclic performance, with PPL/PPS hybrids showing reduced ultimate strength compared to both PPS and PPL fibers. The post-peak behavior of PPL/PPS hybrids resembled that of mono PPS, indicating a detrimental synergistic effect of PPL/PPS hybridization. In contrast, PPL/BF and PPL/PVA hybrids improved post-peak performance compared to mono micro-fibers. The strong chemical bonding of PVA and BF fibers enhanced PPL fiber resilience, preventing pull-out at large deflections and improving the bridging effect and overall load-bearing capacity. PVA fiber dosage notably affected the post-peak behavior of hybrid PPL/PVA systems. The 0.33PPL/0.66PVA hybrid showed a slight increase in ultimate strength and improved post-peak response compared to 0.66PPL/0.33PVA. Moreover, the 0.66PPL/0.33BF hybrid also demonstrated superior post-peak performance, with approximately 74 % higher ultimate strength than the 0.33PPL/0.66BF ratio. This improvement was likely due to the crack-bridging ability of PPL fibers. Higher BF content may enhance cracking strength through its chemical bonding and tensile properties. However, hybridizing with micro-fibers did not enhance the post-peak behavior of single PPL fibers, likely due to insufficient PPL dosage, which limited crack-bridging capacity and reduced load-bearing capacity under high cyclic loads.

3.1.2. Cyclic energy dissipation

The energy dissipation of FR-SWSSC (per cycle and cumulative) is shown in Fig. 9. Compared to FWNS, SWSSC exhibited about 4.3 times higher dissipation at larger deflections, resulting in much higher cumulative energy dissipation by about 93 %. This was likely due to the denser and stronger interlocking of SWSSC (Fig. 6) consistent with previous studies [22, 74, 75]. Micro-fiber incorporation significantly increased low-deflection energy dissipation compared to plain SWSSC. Notably, BF maintained 80 % higher energy dissipation at high deflections compared to plain SWSSC. This potentially resulted from the uniform BF distribution and strong bonding, promoting crack retention at large deformations. PVA fibers exhibited higher energy dissipation compared to BF fibers at low cycles, leading to consistently higher cumulative dissipated energy across all deflection levels. Notably, the PVA-reinforced mixture achieved a maximum cumulative energy dissipation 36 % greater than the plain SWSSC. This enhanced performance could likely be attributed to the strong chemical bonding of PVA fibers, which effectively bridged micro- and macro-cracks. PPL and TPPL fibers surpassed micro-fibers in post-peak energy dissipation, leading to higher cumulative dissipation. PPL fibers were particularly effective, exhibiting 200 % and 82 % greater energy dissipation at large deflections and cumulative dissipated energy, respectively, compared to TPPL fibers. This was likely due to the higher stiffness and improved mechanical bonding

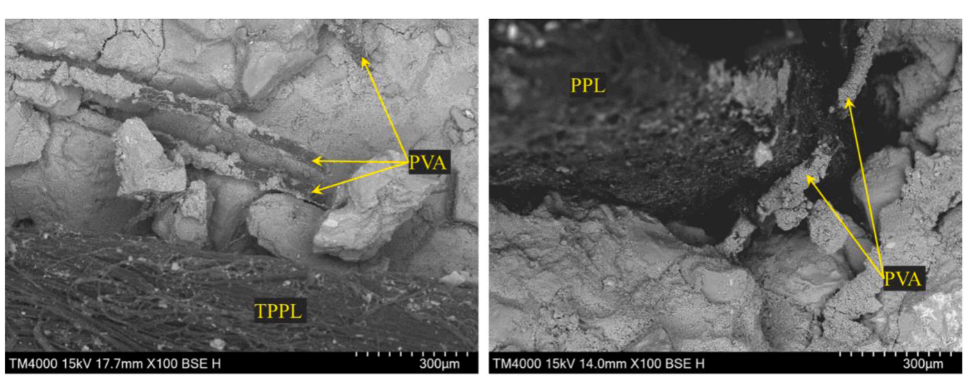

TPPL/PVA PPL/PVA

Fig. 8. Microstructure of PPL/PVA and TPPL/PVA hybridization using SEM images.

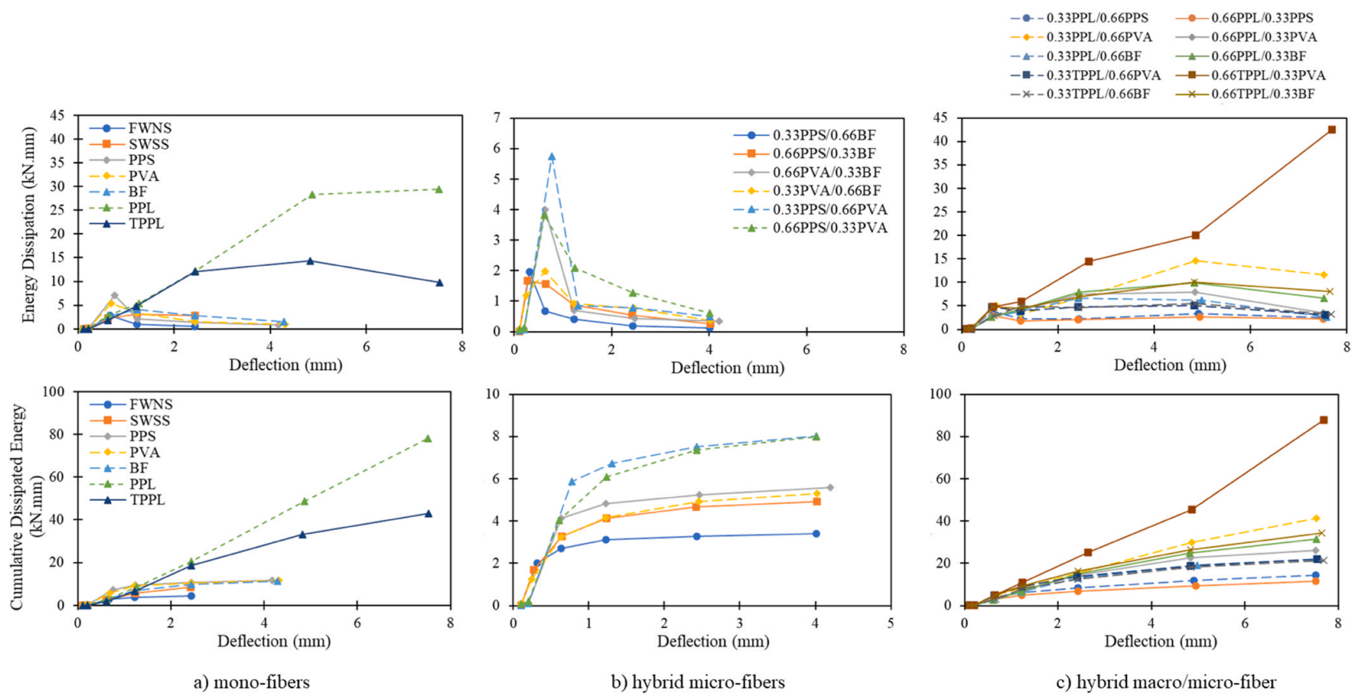

Fig. 9. Energy dissipation of FR-SWSSC mixtures per cycle and cumulative with varying fiber reinforcements: (a) mono-fibers, (b) hybrid micro-fibers, and (c) hybrid macro/micro-fibers.

strength of PPL fibers, which limited macro-crack propagation.

Micro-fiber hybridization in FR-SWSSC decreased energy dissipation compared to mono fibers. While it improved energy dissipation at initial cycles, it reduced energy dissipation for larger deflections across all hybrids. This behavior was likely due to the weak post-peak response of micro-fibers, lacking crack-control and bridging mechanisms, leading to a significant drop in post-peak load-bearing capacity. For example, 0.66PPS/0.33BF resulted in 127 % and 89 % reductions in maximum cumulative energy dissipation compared to mono BF and PPS, respectively. Hybridizing micro/macro-fibers improved micro-fiber energy dissipation. Hybrid 0.33PPL/0.66PVA exhibited significantly higher cumulative energy dissipation than mono PVA fibers at large deflections by about 260 % increase. This approach also yielded an 81 % increase over mono PPL fibers at initial cycles. These findings indicated that PVA fibers were more effective for lower deflection energy dissipation, while PPL fibers benefit larger deflections. PPL/BF hybridization (0.66PPL/0.33BF) exhibited superior energy dissipation, with a 181 % increase in cumulative dissipated energy compared to mono PPL fibers. This was likely due to the lower dosage of BF, mitigating the corrosion concerns of BF reported in previous studies [25,76,77]. While BF corrosion caused reduction in strength and ductility under cyclic loading, a lower dosage could leverage its strong bonding with the concrete matrix to enhance PPL fiber bonding and improve load-bearing capacity at large deflections.

TPPL/PVA hybridization enhanced the energy dissipation capacity at initial cycles. Notably, 0.66TPPL/0.33PVA significantly improved energy dissipation at large deflections compared to both PVA and TPPL fibers. It also resulted in 105 % and 664 % increase in cumulative dissipated energy over TPPL and PVA, respectively. This could be attributed to strong chemical bonding in PVA fibers (Fig. 7), which likely improved TPPL fiber bonding under cyclic loading and strengthened the mix at large deflection cycles. Like PPL/BF hybridization, TPPL/BF at a combination of 0.66TPPL/0.33BF exhibited greater efficacy, likely due to previously reported BF corrosion. This hybrid resulted in 208 % higher cumulative dissipated energy compared to mono BF incorporation.

3.1.3. *Hysteretic damping ratio*

To further investigate the energy dissipation characteristics of FR-SWSSC, hysteretic damping (ξ_{hys}) was evaluated. Hysteretic damping signifies the proportion of energy dissipated relative to the elastic energy stored within the material during deformation. This elastic energy is recovered upon load removal. As defined by [78], hysteretic damping can be expressed as:

$$\xi_{hys} = \frac{1}{4\pi}\frac{E_d}{E_{el}} = \frac{A_l}{\pi F_l d_l} \tag{1}$$

where dissipated energy within the loop is denoted by E_d, while E_{el} represents the elastic strain energy, A_l refers to the area enclosed by the loop, and F_l and d_l correspond to the maximum force experienced by the loop and the deflection associated with that force, respectively.

Fig. 10 demonstrates a significantly higher ξ_{hys} for plain SWSSC compared to FWNS at low deflections by about 67 % increase. This aligns with the denser microstructure observed for SWSSC in Fig. 6. Micro-fiber incorporation (PPS, PVA, BF) further elevated ξ_{hys} by 32 %, 58 %, and 84 % over plain SWSSC at low deflections, likely due to their enhanced crack resistance and energy dissipation properties stemming from strong chemical bonding and tensile strength (particularly PVA and BF). PPL fiber incorporation substantially improved ξ_{hys} (by 160 % vs. plain SWSSC) while TPPL fibers decreased ξ_{hys} at low deflections. This difference was likely attributed to the superior stiffness and mechanical bonding strength of PPL, resulting in greater initial cycle resistance and energy damping. During the initial cycles, TPPL fibers may cause micro-crack development and reduce ξ_{hys} compared to plain SWSSC. However, TPPL fibers still contribute to ξ_{hys} at higher deflections due to their ability to bridge cracks over larger deformations.

Micro-fiber hybridization showed that PPS/BF combinations significantly reduced ξ_{hys}, likely due to the weak bonding of PPS fibers (Fig. 7) and BF corrosion, as reported in previous studies [25, 76, 77], leading to negative synergy. This finding is consistent with previous research on the mechanical properties of PPS/BF hybridizations in SWSSC [25,34]. Conversely, PPS/PVA hybrids exhibited improved ξ_{hys}, with the 0.33PPS/0.66PVA combination resulting in 71 % of ξ_{hys} at low

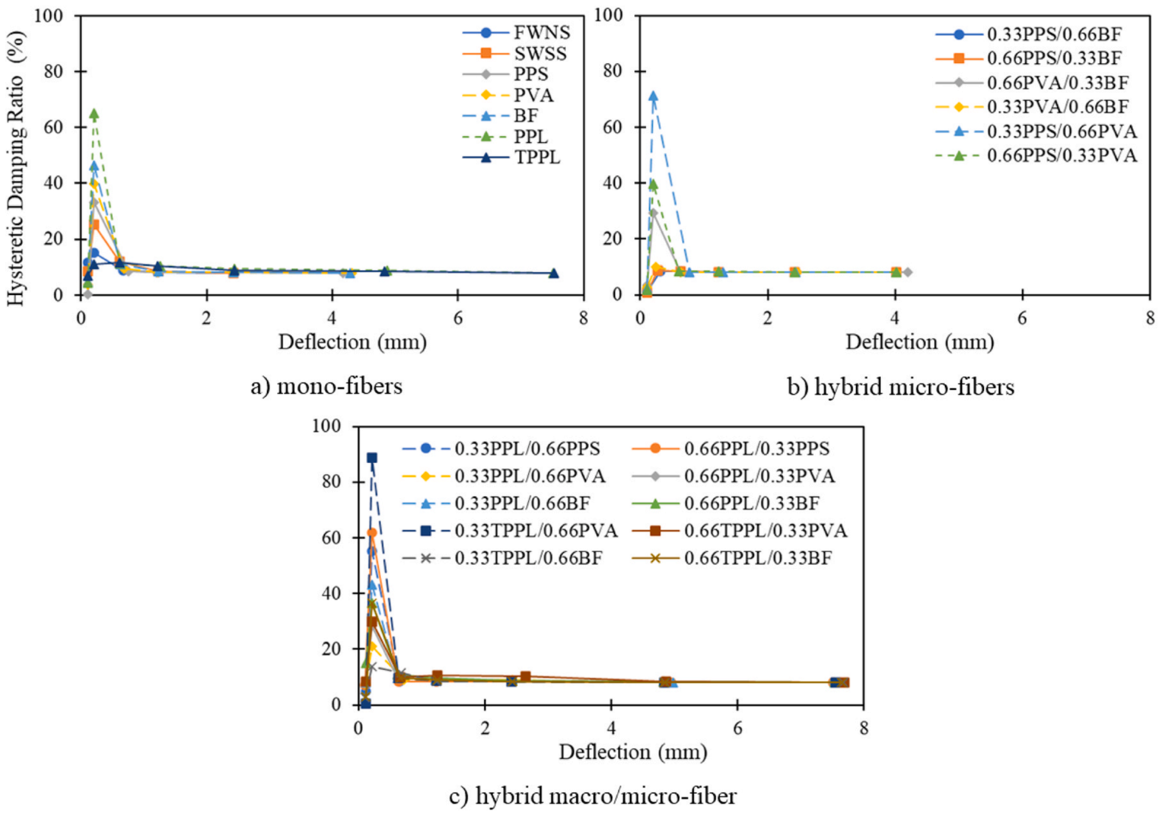

Fig. 10. Hysteretic damping ratio of FR-SWSSC mixtures per cycle with varying fiber reinforcements: (a) mono-fibers, (b) hybrid micro-fibers, and (c) hybrid macro/micro-fibers.

deflections, representing an increase of 79 % and 112 % compared to mono PVA and PPS, respectively. This suggested PVA fibers enhanced PPS fiber bonding within the matrix, leading to greater contribution from PPS fibers in hindering crack initiation and ultimately improving ξ_{hys}. Additionally, the lower stiffness strength of PPS fibers compared to PVA fibers could contribute to elongation and higher strain at failure when bonding was sufficient, further enhancing ξ_{hys}. PVA/BF hybridization decreased ξ_{hys} at low deflections compared to mono PVA and BF. Notably, 0.66PVA/0.33BF exhibited 192 % higher ξ_{hys} than 0.33PVA/0.66BF. Higher BF dosage in the hybrid system might be detrimental due to corrosion. This could lead to brittleness in the BF, thereby impeding its positive interaction with PVA fibers.

Micro/macro-fiber hybridization demonstrated that while mono TPPL fibers exhibited low ξ_{hys}, incorporating TPPL/PVA fibers significantly enhanced it. Notably, 0.33TPPL/0.66PVA hybrid displayed a 123 % and 656 % increase in ξ_{hys} compared to mono PVA and TPPL, respectively. This improvement can be attributed to enhanced TPPL fiber bonding due to PVA addition, alongside improved flexibility, and distribution of TPPL fibers, ultimately leading to more effective energy damping. TPPL/BF hybridization reduced ξ_{hys} compared to mono BF but significantly improved it over mono TPPL fibers. Notably, 0.66TPPL/0.33BF increased ξ_{hys} by 211 % at low deflections compared to mono TPPL fibers. However, increasing BF content in the TPPL hybrid system negatively impacted ξ_{hys}, possibly due to BF corrosion. PPL fiber hybridization with PVA or BF resulted in lower ξ_{hys} compared to mono-fibers. The disparity in PPL and TPPL performance stemmed from the superior fiber distribution of TPPL, leading to a more synergistic interaction with micro-fibers. PPL/PPS hybrids exhibited superior ξ_{hys} compared to mono PPS fibers. Notably, 0.66PPL/0.33PPS and 0.33PPL/0.66PPS composites achieved 84 % and 65 % improvement in ξ_{hys}, respectively, attributed to the ability of PPL fibers to hinder crack initiation and enhance energy damping at lower cycles.

3.1.4. Monotonic vs cyclic flexural behavior

Figs. 11 and 12 depict the contrasting response of FR-SWSSC reinforced with PPL and TPPL fibers and their respective micro-fiber hybrids, under cyclic and monotonic loading. The inherent rigidity and high tensile strength of PPL fibers resulted in superior performance under monotonic conditions. However, cyclic loading led to a deterioration of the PPL fiber-matrix bond, compromising their effectiveness in subsequent cycles. Conversely, TPPL fibers, characterized by flexibility and appropriate bond strength, demonstrated superior performance under cyclic loading. This superior behavior can be attributed to their ability to facilitate efficient stress transfer and effectively bridge micro- and macro-cracks within the concrete matrix.

The partial substitution of PPL fibers with PVA fibers demonstrably improved their cyclic flexural performance. This enhancement could be attributed to the strengthened interfacial bonding facilitated by the incorporation of PVA fibers, ultimately leading to superior behavior under repeated loading and unloading cycles. Moreover, a higher PVA fiber content within the PPL/PVA hybrid system yielded better performance at large deflections. A 66 % substitution of TPPL fibers with PVA resulted in similar load-deflection behavior under both cyclic and monotonic loading regimes. The 0.66TPPL/0.33BF hybrid showed similar performance in both loading conditions. This likely resulted from the strong chemical bonding strength of BF. However, higher BF content significantly reduced the load-bearing capacity after the peak under monotonic loading, possibly due to BF corrosion. PPL/PPS hybrids displayed negligible response modification under monotonic and cyclic loading owing to weak PPS fiber-matrix adhesion. Consequently, increased PPS content resulted in a pronounced post-peak response weakening across both loading regimes.

3.1.5. Energy absorption capacity

To mitigate the risk of catastrophic and abrupt failure under dynamic loading scenarios, such as earthquakes, the incorporation of high-energy

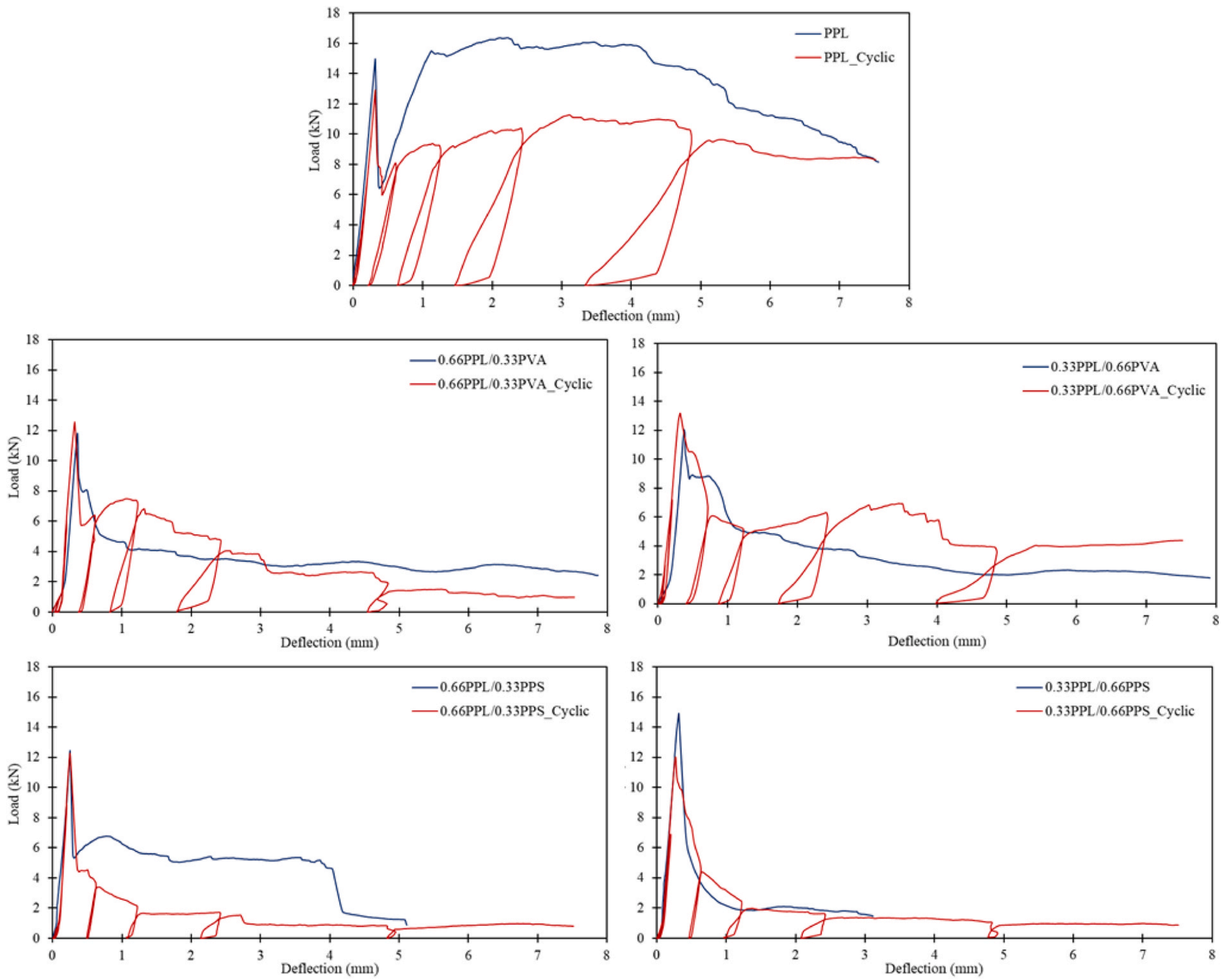

Fig. 11. Monotonic and cyclic load-deflection behavior of FR-SWSSC reinforced with PPL fibers and their hybridization with micro-fibers in flexural testing.

absorption materials becomes a critical design consideration [79, 80]. This study investigated the energy absorption capacity as a key factor influencing the flexural behavior of FR-SWSSC after concrete cracking by using backbone load-deflection results. The energy absorption capacity represents the amount of energy absorbed up to a specific deflection. In this study, T^D_{600} and T^D_{150} were evaluated as employed in previous study [81], representing the energy absorption capacity of FR-SWSSC up to deflection values of 0.50 mm (1/600 of the beam span) and 2 mm (1/150 of the beam span), respectively, as shown in Fig. 13.

Fig. 14 demonstrates that SWSSC exhibited a significantly higher T^D_{150} (by about 67 %) compared to FWNS, while its T^D_{600} is notably lower (by about 64 %). This translated to a ratio of T^D_{150}/T^D_{600} of 5.36 for SWSSC and 1.15 for FWNS. This finding suggested that SWSSC promoted higher energy absorption at post-peak stage, likely due to its denser microstructure and stronger interlocking strength (Fig. 6). Fiber addition significantly enhanced the energy absorption of SWSSC (T^D_{150} and T^D_{600}). This likely stemmed from micro- and macro-fibers bridging cracks at different stages during cyclic loading. While T^D_{150} showed minimal variation with micro-fiber type, PPS fibers yielded a 71 % and 20 % increase in T^D_{600} compared to BF and PVA, respectively. This translated to T^D_{150}/T^D_{600} ratios of 2.03, 2.47, and 3.29 for PPS, PVA, and BF, respectively. The corrosion of BF in SWSSC led to more brittle post-peak behavior and the lowest T^D_{600} among all micro-fibers. PPL and TPPL fiber addition significantly improved post-peak energy absorption, as evidenced by increases of 128 % and 132 % in T^D_{150} for PPL and TPPL, respectively, compared to plain SWSSC. Similarly, T^D_{600} exhibited improvements of 136 % and 32 % for PPL and TPPL, respectively. These findings indicated the effectiveness of macro-fibers in bridging macro-cracks, resulting in a substantial increase in post-peak energy absorption. PPL and TPPL fibers exhibited similar T^D_{150} values, but PPL fibers displayed superior energy dissipation after peak load, resulting in a 79 % higher T^D_{600} value. This difference translated to a T^D_{150}/T^D_{600} ratio of 9.43 for TPPL fibers and 5.19 for PPL fibers. This disparity likely originated from the stronger mechanical bonding in PPL fibers, which mitigated the drop in load-bearing capacity and led to a lower T^D_{150}/T^D_{600} ratio.

Micro-fiber hybridization decreased T^D_{150} but improved T^D_{600} compared to mono-fibers. For example, 0.66PPS/0.33BF hybridization yielded a 12 % increase in T^D_{600} relative to mono BF. This positive synergy likely arises from improved bonding between PPS fibers due to BF incorporation, enhancing their contribution to bridging micro-cracks at low deflection cycles, thereby improving energy absorption. PVA/BF hybridization significantly enhanced T^D_{600} at low deflection cycles, with a 54 % increase observed for 0.66PVA/0.33BF compared to mono BF. This result indicates that after the peak point, the synergy of PVA/BF hybridization improved ductility through the incorporation of PVA fibers, owing to their high tensile strength and strong bond with the concrete matrix. However, micro-fiber hybridization generally increased FR-SWSSC brittleness, although some combinations improved low-deflection performance.

Hybridizing macro/micro-fibers led to significant improvements in T^D_{150} compared to mono micro-fibers. Notably, 0.66PPL/0.33PVA and 0.33PPL/0.66PVA hybrids exhibited 25 % and 39 % higher T^D_{150},

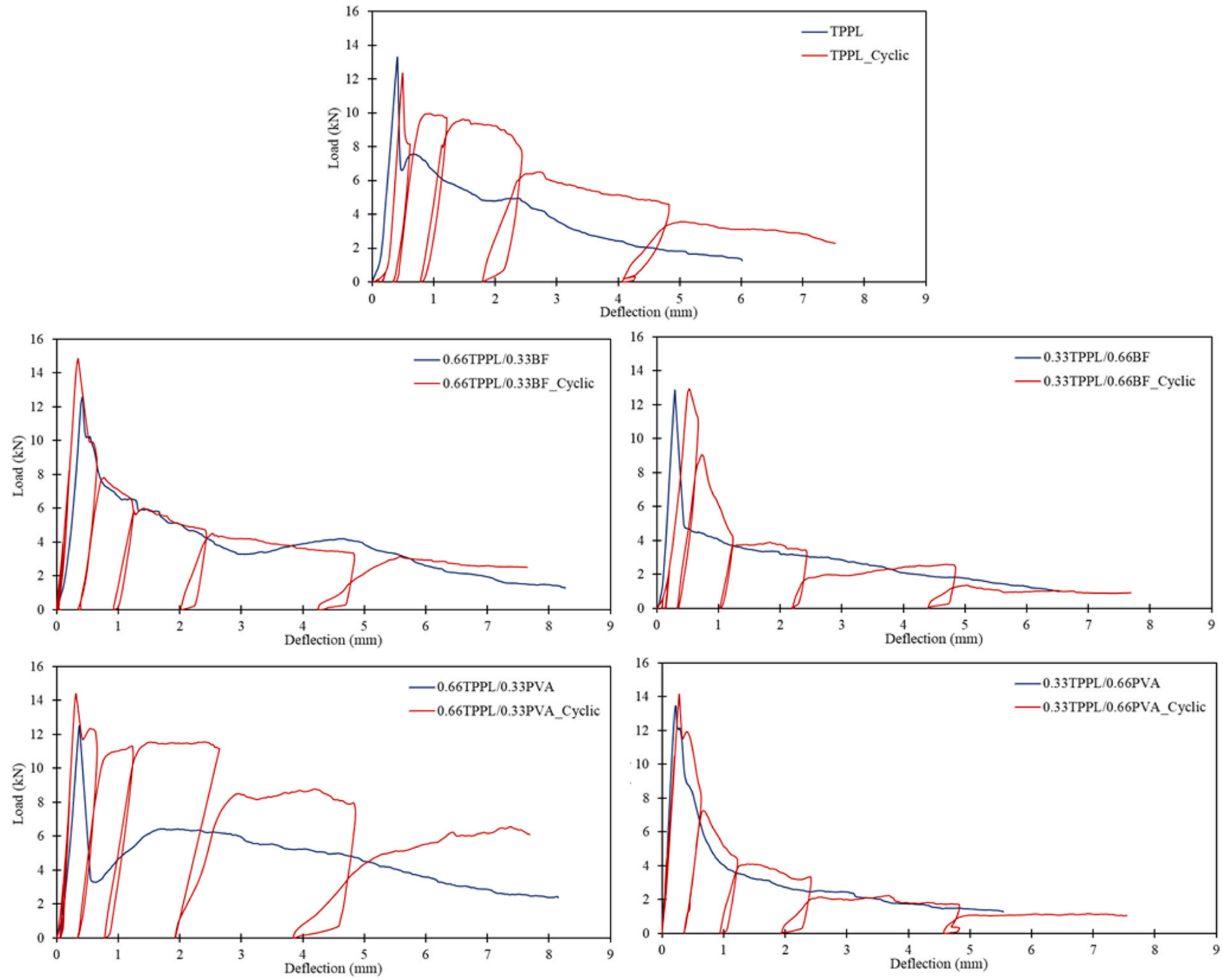

Fig. 12. Monotonic and cyclic load-deflection behavior of FR-SWSSC reinforced with TPPL fibers and their hybridization with micro-fibers in flexural testing.

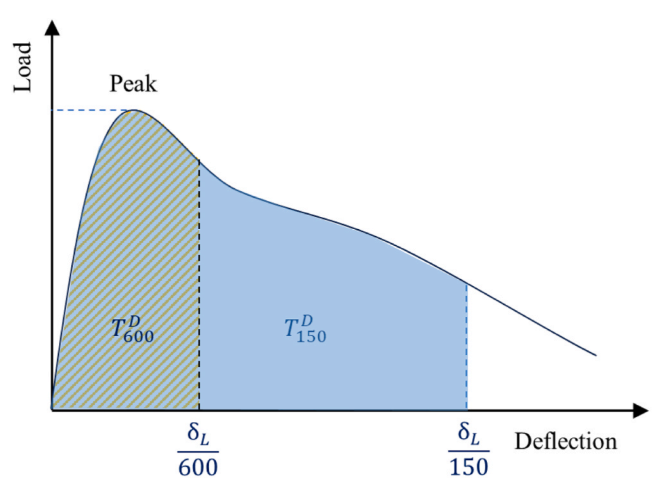

Fig. 13. Characterization of peak load and energy absorption capacity (T^D_{600} and T^D_{150}) in typical backbone load-deflection behavior.

respectively, compared to mono PVA fibers. Similarly, 0.66TPPL/0.33PVA and 0.33TPPL/0.66PVA hybrids achieved 113 % and 28 % enhancements in T^D_{150}, respectively, over mono PVA fibers. T^D_{150} increased by 31 % and 22 % for 0.66PPL/0.33BF and 0.33PPL/0.66BF hybrids, respectively, compared to mono BF fibers. Likewise, 0.66TPPL/0.33BF and 0.33TPPL/0.66BF hybrids exhibited T^D_{150} enhancements of 59 % and 20 %, respectively, compared to mono BF. TPPL fiber hybridization with PVA and BF fibers significantly increased T^D_{600} compared to mono TPPL fibers. Notably, TPPL/PVA hybridization proved more effective, with 0.66TPPL/0.33PVA and 0.33TPPL/0.66PVA exhibiting 155 % and 161 % enhancements in T^D_{600}, respectively, over mono TPPL fibers. This suggests that PVA fibers reinforce micro-cracks, improving low-deflection energy dissipation, while TPPL fibers, due to their superior distribution, bridge macro-cracks, enhancing high-deflection energy absorption. Among macro/micro-fiber hybrids, 0.66TPPL/0.33PVA exhibited the most effective synergy, demonstrating significantly higher energy absorption at both T^D_{150} and T^D_{600} compared to PVA and TPPL mono-fibers.

3.1.6. *Flexural tensile strength*

The flexural tensile behavior of FRC is typically quantified by the equivalent flexural strength ratio, denoted as $R_{e,3}$ [82–84]. This parameter is derived from the energy absorption capacity of FRC up to a deflection corresponding to 1/150 of the beam span and the initial peak load experienced during the flexural test [81, 85–87]. As such, the value of $R_{e,3}$ can be determined through analysis of the backbone load-deflection curves in this study and can be calculated as:

$$R_{e,3} = \frac{T^D_{150}}{P_1 \delta_{L/150}} \quad (2)$$

where P_1 signifies the first peak load.

Fig. 15 depicts the value of $R_{e,3}$ for all mixes and additionally presents the flexural strength at peak and residual, defined as the strength at

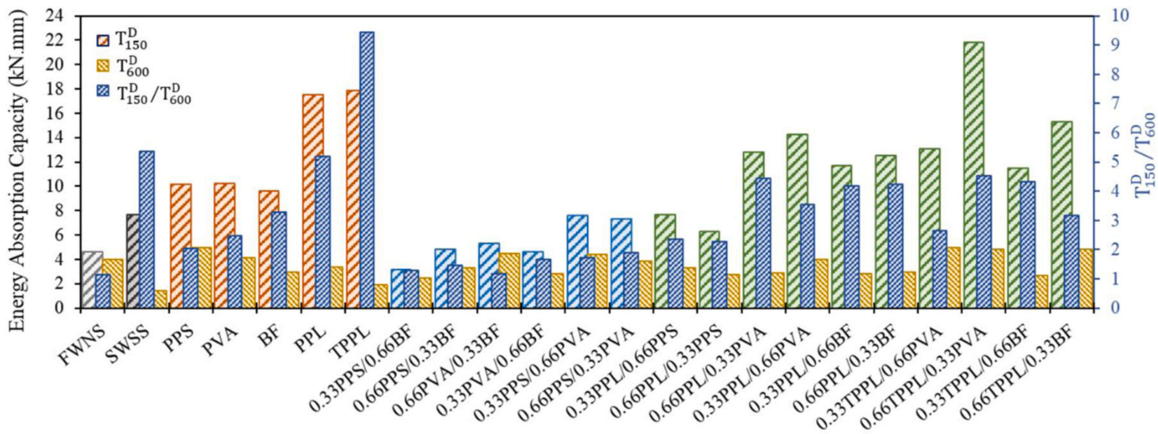

Fig. 14. Energy absorption parameters of FR-SWSSC mixtures from backbone curves.

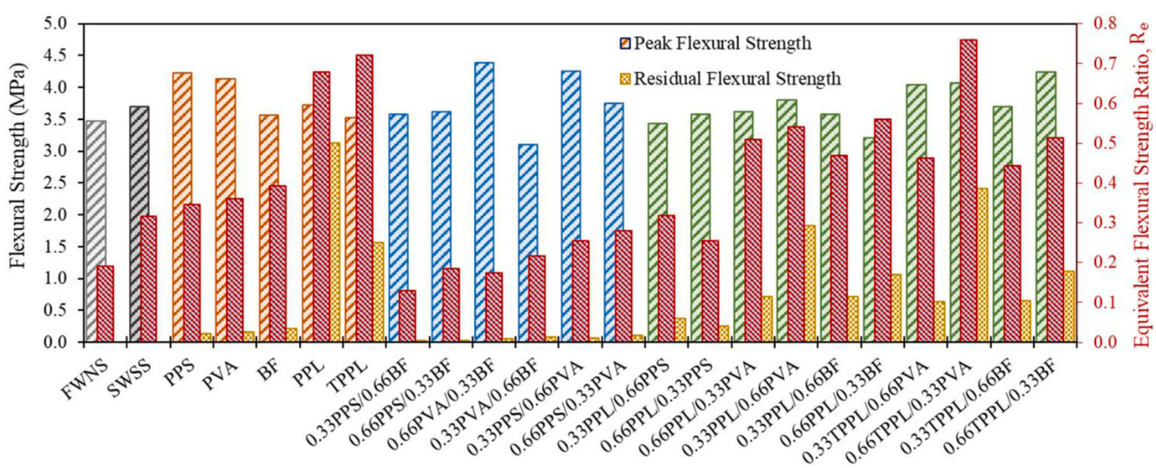

Fig. 15. Flexural strength, residual strength, and equivalent flexural strength of all mixtures.

3.5 mm deflection. Eq. 3 was employed to calculate both peak and residual flexural strength. According to ASTM C1609 standard [87], the first peak strength was identified as the cracking strength of FR-SWSSC.

$$f_u = \frac{P_u L}{bd^2} \tag{3}$$

where L, b, and d denote the span, width, and depth of the beam specimen, respectively.

Plain concrete mixes (FWNS and SWSSC), lacking fibers and exhibiting brittle behavior, displayed no residual flexural strength. SWSSC exhibited 68 % greater $R_{e,3}$ compared to FWNS. This aligns with other study results, suggesting that the denser microstructure of SWSSC and superior interlocking contribute to its enhanced flexural strength. Compared to plain SWSSC, micro-fibers marginally improved residual flexural strength. Macro-fibers, however, achieved significantly higher residual strength due to crack bridging and energy absorption. PPL fibers were more effective (99 % higher strength than TPPL), possibly due to their stiffness and appropriate bond with the matrix. Conversely, TPPL fibers exhibited a 6 % increase in $R_{e,3}$ compared to PPL fibers, likely due to their enhanced energy absorption capability facilitated by their flexibility. Furthermore, BF demonstrated the highest $R_{e,3}$ among the micro-fibers, exceeding plain SWSSC by 22 %.

Micro-fiber hybridization decreased residual flexural strength and $R_{e,3}$ compared to mono micro-fibers. However, cracking strength in FR-SWSSC exhibited some improvement with hybridization, with 0.66PVA/0.33BF achieving 6 % and 23 % increases over mono-PVA and BF, respectively. This suggested a positive synergy from PVA/BF hybridization, potentially due to BF enhancing PVA fiber bonding and consequently improving cracking strength. Macro/micro-fiber hybridization significantly increased residual flexural strength and $R_{e,3}$ compared to mono micro-fibers. For example, 0.33PPL/0.66PVA hybrid exhibited 10.8 times greater residual flexural strength and 50 % higher $R_{e,3}$ than mono PVA fibers. Also, 0.66PPL/0.33BF hybridization yielded 382 % and 44 % higher residual flexural strength and $R_{e,3}$, respectively, compared to mono BF. This improvement was attributed to the ability of PPL fibers to bridge macro-cracks and enhance energy absorption. Interestingly, for PPL fiber hybridization, PVA was more effective at higher dosages, while the opposite was true for BF. This disparity was likely due to BF corrosion in SWSSC, leading to brittleness [25, 77, 88]. Therefore, lower BF content resulted in superior flexural performance when combined with PPL fibers. Moreover, the hybrid PPL/PPS fibers exhibited slightly higher residual strength than mono PPS fibers, attributed to the crack-bridging effect of PPL fibers. However, when the fiber dosage was reduced in the hybrid mix, the $R_{e,3}$ value decreased compared to both mono PPS and PPL fibers. This suggests a negative synergy and the inability of the fibers to complement each other effectively, likely due to the lower bonding strength of PPS and the reduced stiffness of PPL, negatively impacting stress distribution and flexural performance.

0.66TPPL/0.33PVA hybrid displayed a 54 % and 15 % increase in residual flexural and cracking strengths, respectively, compared to mono TPPL fibers. $R_{e,3}$ also improved by 6 % and 111 % for the hybrid relative to mono TPPL and PVA, respectively. This synergy was attributed to the strong interaction of PVA fibers with the concrete matrix, enhancing TPPL fiber bonding and promoting energy dissipation for improved flexural strength. Previous study on the hybridization of macro-BF and micro PVA fibers revealed similar results in FWNS concrete, indicating that a higher percentage of macro-BF was more effective under cyclic loading [89]. 0.66TPPL/0.33BF hybridization yielded a 20 % increase in cracking strength compared to mono TPPL fibers. This enhancement was attributed to the ability of BF to improve TPPL fiber bonding strength. However, increasing the BF content resulted in a detrimental effect due to corrosion.

3.2. Damage characteristics

An evaluation of FR-SWSSC damage was conducted using damage index (DI), strength deterioration ratio (SDR), and degree of reversibility (R). These parameters were determined using Eqs. (4) to (6) from the data presented in Fig. 16.

$$DI_i = 1 - E_{d_i}/E_0 \tag{4}$$

$$SDR_i = P_{rel_i}/P_{unl_i} \tag{5}$$

$$R_i = 1 - D_{residual_i}/D_{\max_i} \tag{6}$$

where E_{d_i} and E_0 denote the damage modulus and initial modulus, respectively. P_{rel_i} represents the reloading strength, and P_{unl_i} signifies the unloading strength. Additionally, $D_{residual_i}$ and $D_{\max_i}$ correspond to the residual deflection and maximum displacement experienced during each loading cycle (i). The results of the investigated damage parameters—DI, SDR, and R—are presented in Figs. 17 to 19. The DI represents the reduction in concrete stiffness during unloading, caused by damage. The SDR value obtained from the cyclic flexural test provides a quantitative measure of the cyclically induced reduction in the load-bearing capacity during loading-unloading cycles. A lower SDR value corresponds to a more significant loss in capacity. The R factor signifies the degree of elastic recovery of concrete after a loading-unloading cycle. This reflects the resilience of concrete under repeated bending stresses. Higher R values indicate greater reversibility, suggesting more elastic behavior and improved performance under cyclic loading due to reduced permanent deformation with each cycle.

3.2.1. Plain concrete

The DI results for plain concrete mixes showed that both SWSS and FWNS exhibited similar damage indices across cycles, with FWNS having a slightly higher DI at deflections exceeding 1 mm. FWNS consistently exhibited up to 20 % higher SDR than SWSS across all deflections. However, FWNS showed a higher R value at deflections below 0.4 mm, while SWSS outperformed FWNS at greater deflections. These results suggest that at lower deflections, the presence of salts in SWSS induced micro-cracks in the early cycles, exacerbated by its denser, more brittle microstructure [22, 74, 75]. This led to higher residual deflections (lower R) and greater strength reduction (lower SDR) compared to FWNS. At higher deflections, the increased interlocking strength in SWSSC resulted in more reversibility and less residual deformation, leading to more elastic behavior than FWNS. Although crack propagation reduced SDR, the preserved elasticity led to slightly lower stiffness degradation and DI in SWSS. Conversely, FWNS exhibited higher ductility due to the absence of salts, promoting distributed micro-cracking, which resulted in a higher SDR but lower R.

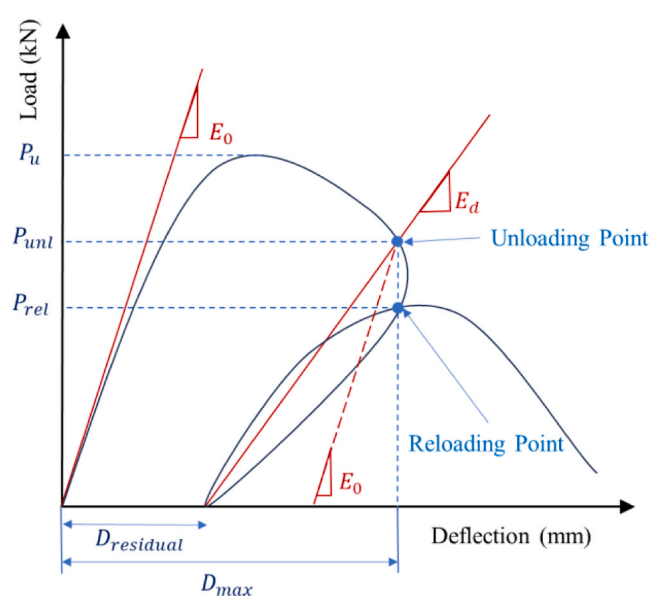

Fig. 16. Cyclic damage parameters.

3.2.2. Mono-fibers

Mono micro-fibers primarily affected the early loading cycles due to their limited ability to bridge macro-cracks after peak strength, constrained by their short length. Their addition significantly improved the SDR of SWSSC by enhancing micro-crack bridging and reducing strength loss. PPS fibers increased both SDR and R values at deflections below 0.5 mm; however, beyond this point, the R value dropped sharply. This suggests that PPS fibers provided elastic recovery (high R) and retained strength (high SDR) at small deflections due to their better distribution, which improved the elastic modulus and initial stiffness. However, weak bonding with the concrete matrix and low tensile strength led to fiber pull-out after the peak deflection (0.3 mm), limiting crack bridging at larger deflections and causing reductions in both SDR and R for deflections above 0.5 mm. PVA fibers, with superior chemical bonding, maintained higher SDR at larger deflections, indicating better strength retention during cyclic loading. The R value for PVA fibers was comparable to PPS, likely due to similar stiffness and elastic modulus, resulting in similar elastic behavior and residual deflections at larger deflections. Conversely, BF of PPS and PVA reinforced SWSSC, with its higher elastic modulus and strong bond with the matrix, provided better reversibility and higher R at large deflections, leading to lower residual strength. This contributed to the lowest SDR among all mono micro-fibers, likely due to the elastic behavior and low elongation BF, resulting in reduced strength retention. Consequently, BF showed a similar DI to plain SWSSC. PPS and PVA fibers, while improving initial stiffness, caused higher DI at all deflections. After peak deflection (approximately 0.3 mm for PPS and 0.4 mm for PVA), both fibers experienced a sharp drop in stiffness after crack formation, leading to greater DI due to the increased difference between unloading and initial stiffness.

The incorporation of PPL fibers resulted in a significantly higher DI than TPPL fibers at all deflections, and outperformed plain SWSSC for deflections below 1.2 mm. This is likely due to the better distribution and flexibility of TPPL fibers, which helped preserve initial stiffness during loading-unloading cycles, leading to a lower DI compared to PPL and plain SWSSC. Conversely, PPL fibers demonstrated higher SDR and R values across all deflections compared to TPPL fibers. Notably, PPL fibers improved SDR by 22 % at low deflections, attributed to their superior mechanical bonding and stiffness, which minimized strength reduction and residual deflections. Both PPL and TPPL fibers enhanced SDR for deflections below 0.9 mm, likely due to crack bridging by macro-fibers. Regarding deflection reversibility, TPPL fibers resulted in lower R values than plain SWSSC for deflections below 0.9 mm, while PPL fibers exhibited higher R. However, for deflections exceeding 0.9 mm, both fiber types showed higher R values than plain SWSSC, likely due to the flexibility of TPPL, causing early micro-crack formation, leading to initial residual deflection. At larger deflections, the crack-bridging ability of TPPL fibers reduced residual deflections and increased R values.

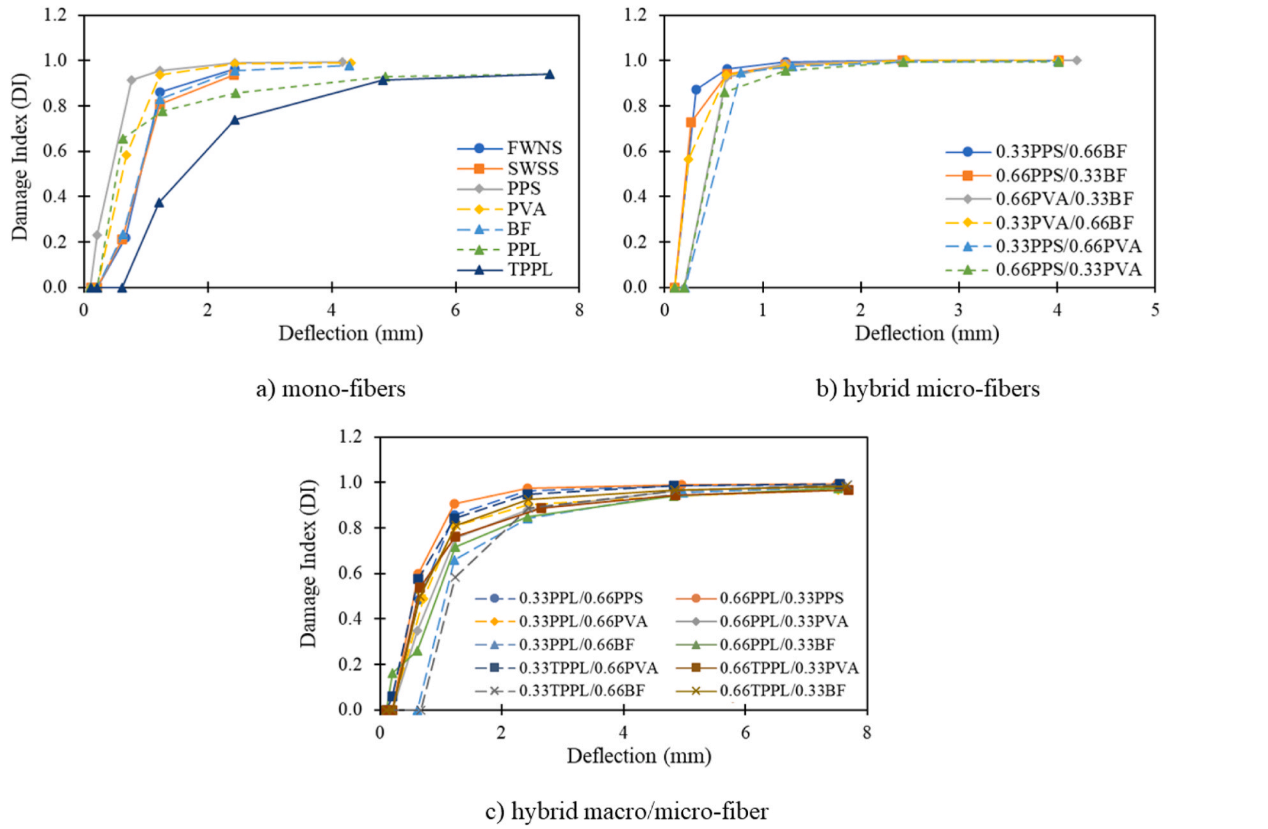

Fig. 17. Damage index (DI) of FR-SWSSC mixtures per cycle with varying fiber reinforcements: (a) mono-fibers, (b) hybrid micro-fibers, and (c) hybrid macro/micro-fibers.

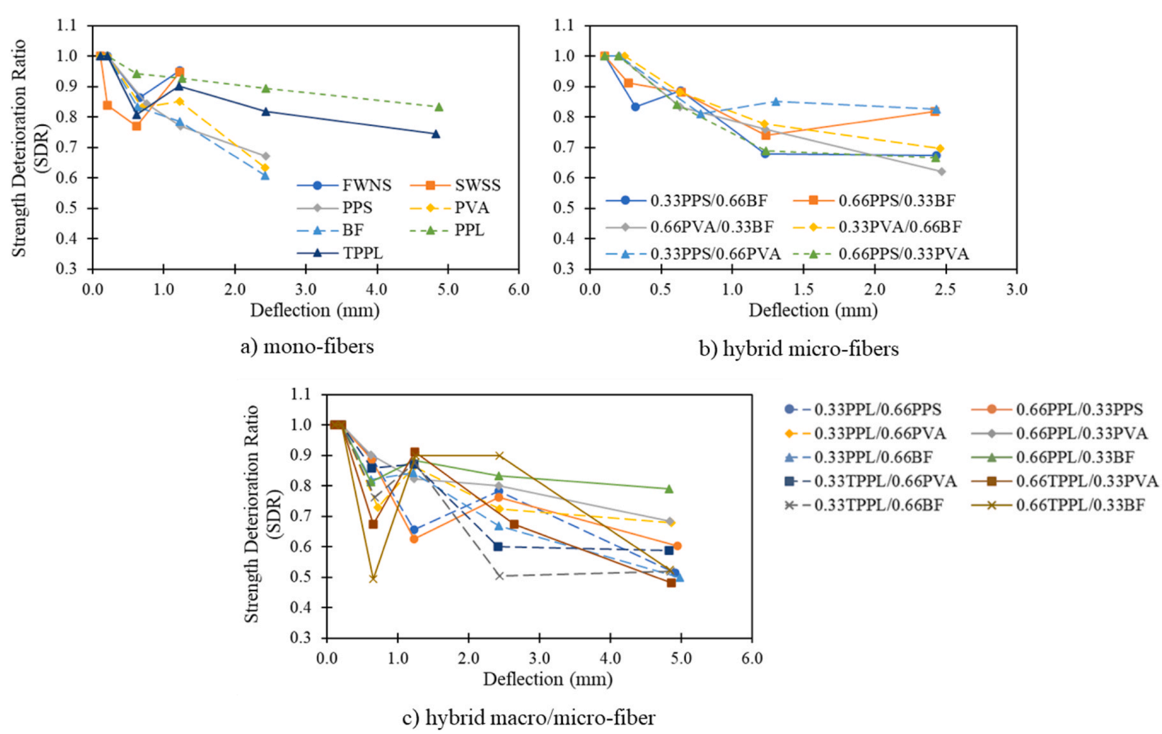

Fig. 18. Strength degradation ratio (SDR) of FR-SWSSC mixtures per cycle with varying fiber reinforcements: (a) mono-fibers, (b) hybrid micro-fibers, and (c) hybrid macro/micro-fibers.

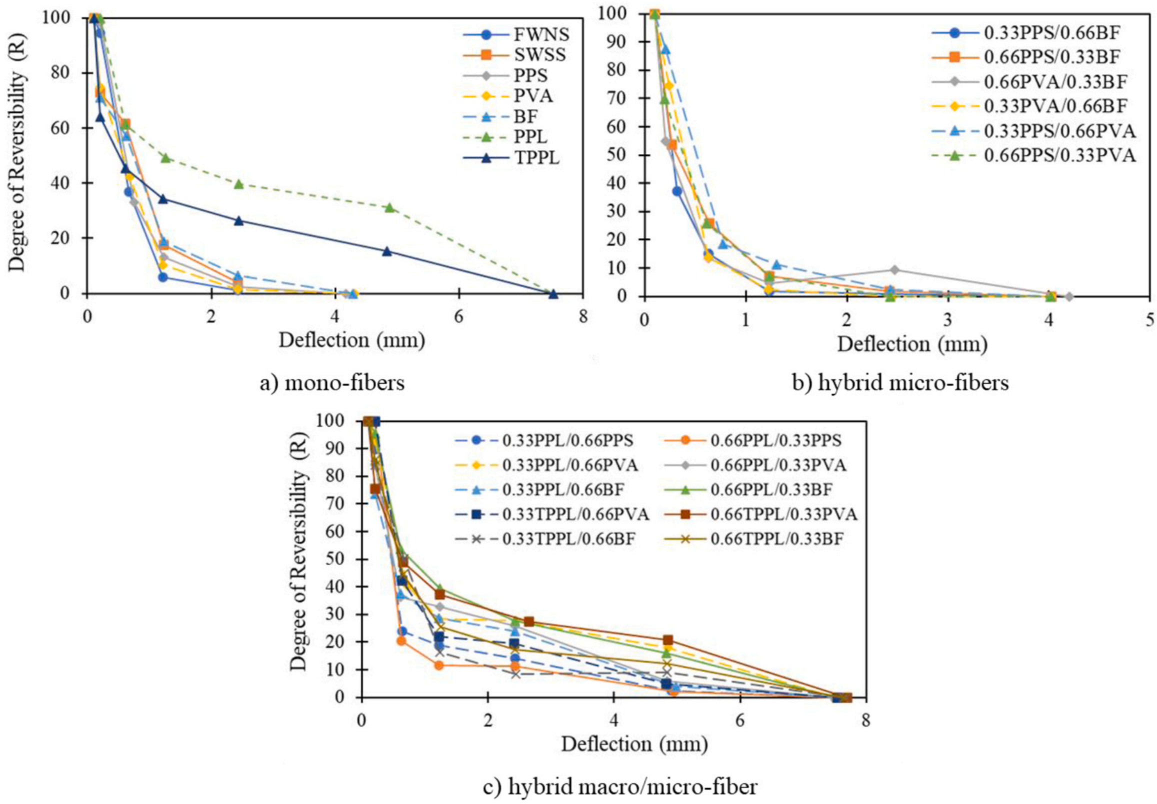

Fig. 19. Degree of reversibility (R) of FR-SWSSC mixtures per cycle with varying fiber reinforcements: (a) mono-fibers, (b) hybrid micro-fibers, and (c) hybrid macro/micro-fibers.

3.2.3. Micro-fiber hybridization

Micro-fiber hybridization showed that PPS/BF and PVA/BF hybrids outperformed mono fibers in DI, particularly at low deflection cycles. This can be attributed to BF increasing the initial stiffness of the hybrid systems with PPS and PVA fibers, resulting in more elastic behavior and increased brittleness. Consequently, the peak deflection decreased, followed by a sharper drop in the hybrids containing BF. The synergy of BF with PPS and PVA fibers led to higher DI at low deflections compared to mono PPS and BF, reducing residual deflection and R values in PPS/BF and PVA/BF hybrids. The 0.66PPS/0.33BF hybrid exhibited greater R than 0.33PPS/0.66BF, likely due to BF corrosion in SWSSC, which reduced ductility. The 0.66PVA/0.33BF hybrid achieved superior R values at higher deflections compared to mono PVA and BF, as hybridization improved concrete ductility. BF enhanced PVA fiber bond strength, allowing full utilization of tensile capacity. The 0.33PVA/0.66BF hybrid showed better SDR at low deflections than mono PVA and BF, and at higher deflections compared to BF. This result indicated positive synergy which improved interlocking in SWSSC and strength recovery across all deflections. While a higher BF dosage aided strength recovery, PVA content improved elasticity compared to mono BF. In PPS/BF hybrids, the 0.66PPS/0.33BF hybrid was more effective for strength recovery, showing 22 % and 35 % higher SDR than mono PPS and BF. In PPS/PVA hybrids, the 0.33PPS/0.66PVA combination performed better, with lower DI at low deflections compared to mono PPS, improved R at large deflections, and reduced residual deflection. This effect can be attributed to a synergistic mechanism: PVA fibers bridged initial cracks, while the lower modulus of PPS facilitated uniform stress distribution, delaying damage, and improving cracking strength (Fig. 15). This synergy also enhanced high-deflection SDR and load-bearing capacity during loading-unloading cycles, with the hybrid 0.33PPS/0.66PVA mix showing a 23 % and 30 % increase in SDR at failure compared to mono PPS and PVA, respectively.

3.2.4. Macro/micro-fiber hybridization

The PPL/PPS hybrid exhibited a lower DI at low deflections compared to both mono PPL and PPS, and reduced DI relative to PPS at the post-peak stage, suggesting a synergistic effect in preventing initial micro-cracks and lowering early damage. The mechanical bonding and stiffness of PPL fibers helped preserve initial stiffness and reduced damage across all deflections compared to PPS, which showed stiffness degradation during cyclic loading. This effect was more pronounced in the 0.33PPL/0.66PPS combination. PPL/PPS hybridization also led to a 17 % increase in SDR over mono PPS at 2.4 mm (the failure point for PPS), though it resulted in a 19 % decrease in SDR at 1.2 mm in the post-peak stage. The pull-out of PPL fibers during large crack development at post-peak reduced strength recovery and SDR, but at higher deflections, PPL fibers more effectively bridged larger cracks, maintaining strength better than mono PPS fibers.

A higher proportion of PPL fibers led to significantly greater strength recovery and SDR than PPL/PPS hybridization, highlighting the importance of macro-fiber dosage for maintaining strength during loading-unloading cycles. This trend was reflected in the R values, with mono PPL showing lower residual deflection than PPL/PPS. PPL/PPS hybridization also increased the R value compared to mono PPS at deflections over 1.2 mm, showing positive synergy in crack bridging and deflection recovery by PPL fibers. A similar effect was observed in PPL/PVA hybridization, which improved R values compared to PPL/PPS, attributed to enhanced bonding strength between PPL and PVA fibers and their positive synergy. The synergistic crack-bridging by PVA (micro-cracks) and PPL (macro-cracks) improved ductility and reversibility. This effect also resulted in higher SDR values than mono PVA fibers at large deflections, particularly with a 0.66PPL/0.33PVA combination, showing a 26 % increase at 2.4 mm compared to 14 % for 0.33PPL/0.66PVA. PPL/PVA hybridization maintained initial stiffness better, reducing damage and stiffness degradation compared to mono PVA. It also resulted in lower DI than mono PPL at deflections below

1.2 mm, likely due to improved bonding and stress distribution from PVA fibers, which reduced PPL fiber pull-out and subsequent damage.

The hybridization of PPL and BF fibers resulted in a lower DI compared to mono-fiber inclusions, with the 0.33PPL/0.66BF ratio being most effective at lower deflection cycles. This partial replacement improved concrete strength during crack initiation and propagation. The SDR showed strong dependence on fiber content, with 0.66PPL/0.33BF offering a 37 % higher SDR than mono BF at 2.4 mm deflection (failure point of BF), while 0.33PPL/0.66BF showed a 10 % improvement. Additionally, 0.66PPL/0.33BF provided a 59 % increase in SDR compared to 0.33PPL/0.66BF, likely due to the synergy between PPL and BF. BF enhanced the bonding strength of PPL, improving the ability of the system to recover strength through the fiber bridging of PPL fibers in large cracks. This effect was also evident in deflection recovery, with 0.66PPL/0.33BF proving more effective, leading to lower residual strength and higher R than mono BF. However, increased BF content, due to its susceptibility to corrosion, resulted in greater brittleness and reduced strength recovery and SDR under cyclic loading.

Hybridizing TPPL with PVA or BF resulted in less damage than mono micro-fibers (PVA or BF) but more than mono TPPL. At 1.2 mm deflection, 0.66TPPL/0.33PVA and 0.33TPPL/0.66PVA increased DI by 103 % and 125 % compared to mono TPPL, while reducing it by 18 % and 10 % relative to mono PVA. This was likely due to PVA fibers enhancing the initial stiffness of the hybrid system. The TPPL/PVA synergy improved low-cycle SDR, particularly for 0.33TPPL/0.66PVA, compared to mono fibers. However, at higher deflections (2.4 mm), 0.66TPPL/0.33PVA showed superior load-bearing capacity, increasing SDR by 12 % compared to 0.33TPPL/0.66PVA, likely due to PVA strengthening the TPPL bond. Additionally, 0.66TPPL/0.33PVA hybridization improved deflection recovery and increased R values compared to both mono TPPL and PVA, attributed to better crack bridging, lower residual deflection, and more elastic behavior due to

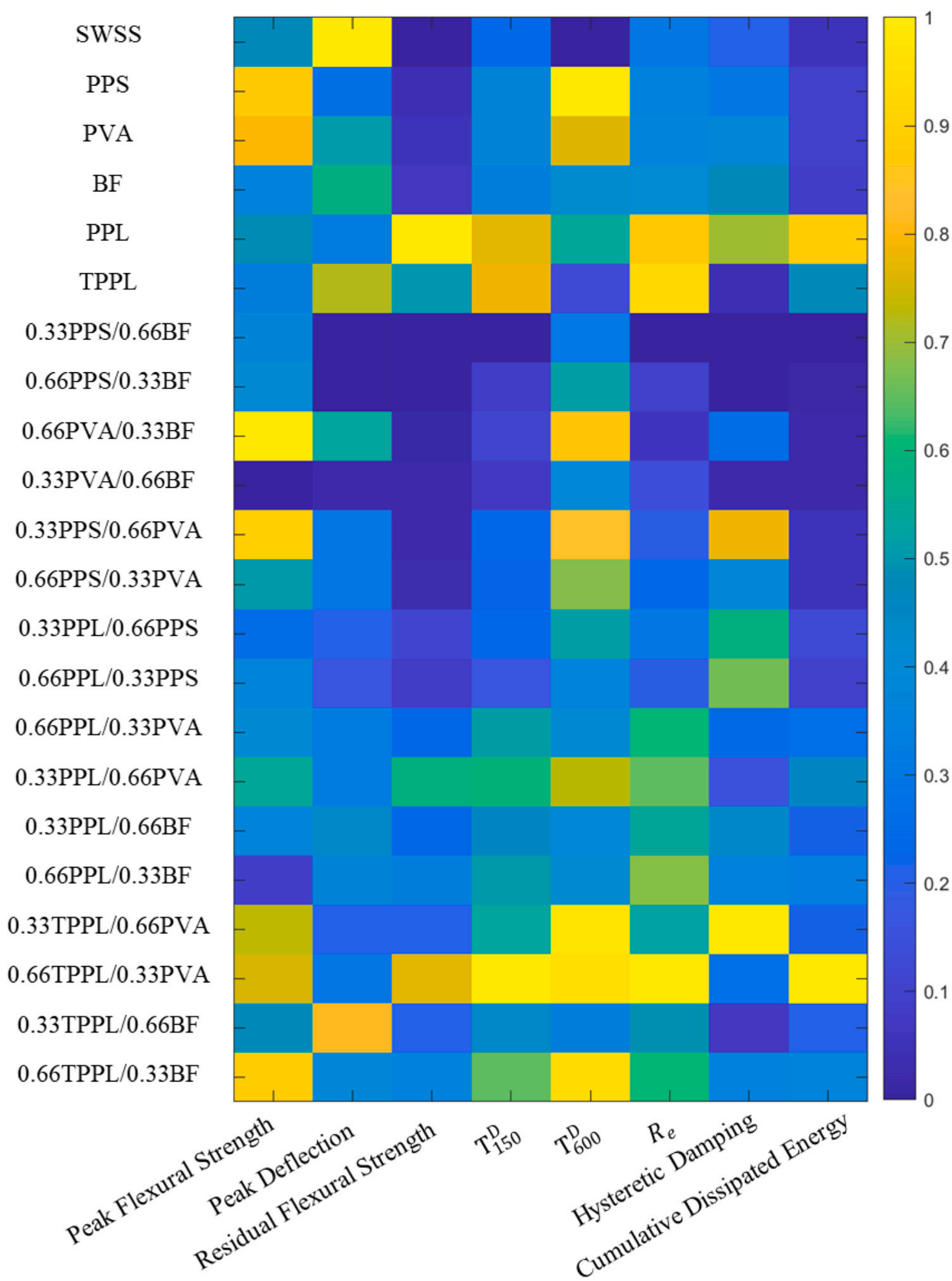

Fig. 20. Heatmap of all investigated normalized parameters for different hybrid FR-SWSS mixes.

PVA inclusion.

The hybridization results of TPPL/BF showed that a lower BF content (0.66TPPL/0.33BF) was more effective, due to the brittleness caused by BF corrosion. At deflections greater than 1.2 mm, this mix exhibited higher SDR and R values, likely due to improved bonding strength of TPPL fibers. The presence of 0.33BF promoted more elastic behavior after peak load, allowing TPPL fibers to bridge cracks more effectively, leading to higher SDR and R compared to mono BF. This elastic response, coupled with greater initial stiffness than mono TPPL or BF, resulted in higher DI in low-cycle conditions. At 2.4 mm deflection, 0.33TPPL/0.66BF increased DI by 20 % and decreased it by 7 % compared to mono TPPL and BF, respectively.

In macro/micro-fiber hybridization, a higher dosage (66 %) of macro-fibers resulted in lower SDR due to their superior bridging ability. Micro-fibers with chemical bonding properties, such as PVA and BF, enhanced performance, with PVA excelling at low deflections and BF at the post-peak stage. Hybrid macro/micro-fiber showed higher R values than mono micro-fibers but lower than mono macro-fibers in the post-peak stage. Notably, 0.66PPL/0.33BF had the highest R value for deflections below 2.0 mm, while 0.66TPPL/0.33PVA dominated above 2.0 mm.

4. Summary and conclusion

This study explored the impact of hybrid fiber reinforcement on the cyclic flexural response of fiber-reinforced seawater sea-sand concrete (FR-SWSSC). Five distinct fiber types were employed: micro-PPS, PVA, and BF alongside macro-PPL and TPPL. All fiber types were incorporated at a constant volume fraction of 0.25 %. These fibers were incorporated into plain SWSSC in various combinations, including mono-fibers, hybrid micro-fibers, and hybrid micro-macro fiber configurations, to evaluate the synergistic effect of hybridization. The results elucidate the ability of hybrid fibers to improve the cyclic performance of FR-SWSSC. Fig. 20 and Table 3 summarize the results of the parameters for all investigated mixtures, highlighting the synergistic effects of fibers in the hybrid systems and offering further clarification of the findings. Fig. 20 presents a heatmap of the various parameters analysed, normalized to the maximum value, resulting in a ratio ranging from 0 to 1.0. Based on the experimental observations, the following conclusions can be drawn:

- Micro-fibers enhanced the load-bearing capacity and minimized residual deflection at low deflections and initial cycles, with PPS fibers outperforming others. PPS fibers exhibited significantly higher energy dissipation (71 % and 20 % compared to BF and PVA) at 1/600th beam deflection, likely due to their micro-crack bridging and elongation capabilities. Conversely, PVA and BF displayed higher hysteretic damping at low deflections due to strong chemical bonds.
- Macro-fibers enhanced post-peak behavior, particularly during large deflection cycles, by bridging macro-cracks. PPL fibers exhibited significantly superior performance compared to TPPL fibers, with increases of 82 % in cumulative energy dissipation, 99 % in flexural strength, and 160 % in hysteretic damping. This likely stemmed from the stiffness and mechanical bonding strength of PPL fibers. However, TPPL fibers demonstrated a significant reduction in damage index across all cycles, potentially due to their improved distribution and flexibility.
- Micro-fiber hybridization improved energy dissipation during initial cycles compared to mono-fibers, due to their complementary effects. However, micro/macro-fiber hybridization resulted in a more significant improvement during large deflection cycles, which can be attributed to their synergistic ability to bridge large cracks.
- In PPS/PVA hybrids, a positive synergy was observed, with PVA fibers bridging initial cracks while the lower modulus of PPS facilitated uniform stress distribution, delaying damage, and improving cracking strength. The 0.33PPS/0.66PVA combination performed better, exhibiting a lower damage index at low deflections compared to mono PPS and reduced residual deflection. It also increased the hysteretic damping ratio by 79 % and 112 % at low deflections, compared to mono PVA and PPS fibers, respectively.
- The 0.66TPPL/0.33PVA hybrid improved deflection recovery and increased cumulative energy dissipation by 105 % and 664 % over mono TPPL and PVA, respectively. Moreover, 0.33TPPL/0.66PVA improved hysteretic damping by 123 % and 656 % compared to mono PVA and TPPL, respectively. This improvement resulted from the enhanced bonding of TPPL by PVA, which strengthened the concrete matrix, improved crack bridging, reduced residual deflection, and promoted more elastic behavior.
- PPL/PVA hybridization indicated that the 0.33PPL/0.66PVA hybrid showed a slight increase in ultimate strength and improved post-peak response compared to 0.66PPL/0.33PVA. Additionally, the 0.33PPL/0.66PVA hybrid provided a 39 % increase in energy dissipation at 1/150th beam deflection, a 260 % improvement in cumulative energy dissipation, and 10.8 times greater residual flexural strength than mono PVA fibers.
- A lower dosage of BF in a hybrid system with micro- or macro-fibers resulted in superior cyclic performance compared to higher BF content. This improvement was attributed to the corrosion of BF in SWSSC, which led to increased brittleness. Conversely, incorporating higher dosage of PVA fibers in the hybrid system also led to better

Table 3
The synergistic actions of fibers in the hybrid system of FR-SWSSC.

Groups	Hybrid FR-SWSSC mixes	Synergistic actions
Hybrid micro	PPS/PVA	– The synergy between PVA and PPS fibers enhanced bonding, crack prevention, and strength, with uniform stress distribution improving cracking strength. – Lower modulus of PPS promoted uniform stress distribution, delaying damage.
	PPS/BF	– BF incorporation improved the bonding strength of PPS fibers. – Synergistic effect enhanced PPS contribution to bridging micro-cracks at low deflection cycles. – Higher BF dosage had a negative effect, likely due to BF corrosion in SWSSC.
	PVA/BF	– Synergistic effect of PVA/BF improved bonding strength and elastic modulus, resulting in higher strength. – BF enhanced PVA fiber bond strength, enabling full utilization of tensile capacity.
Hybrid macro/micro	PPL/PPS	– PPL fibers effectively hinder crack initiation. – PPL fibers enhanced energy damping during lower cycles.
	PPL/PVA	– Enhanced bonding of PPL fibers was likely due to PVA addition. – Greater dosage of micro-fibers in the hybrid system was more effective. – Synergistic effect, maintained load-bearing capacity during cyclic loading.
	PPL/BF	– The chemical strength of BF improved the bonding strength of PPL fibers by reinforcing its surrounding matrix. – PPL fiber inclusion improved the performance of BF.
	TPPL/PVA	– TPPL fibers bridged macro-cracks; PVA fibers reinforced micro-cracks and improve bond strength of TPPL fibers. – Positive synergy increased the performance of PVA fibers, enhancing flexural strength, reducing damage, lower residual deflection and improving elastic behavior.
	TPPL/BF	– Higher BF content negatively affected hybrid system performance, likely due to corrosion. – Synergistic effect improved performance through enhanced TPPL fiber bonding. – BF fibers were effective post-peak but reduced ductility.

cyclic performance, likely due to the high chemical bonding strength of PVA fibers.

This study explored the application of fiber hybridization in SWSSC and revealed its potential to enhance cyclic flexural performance. This improvement was attributed to synergistic effects within the hybrid fiber configuration. These findings suggest the suitability of hybrid FR-SWSSC for structures exposed to cyclic loading, such as those in coastal and offshore environments. The use of hybrid fibers improves ductility, energy dissipation, and crack control, resulting in more resilient and sustainable coastal structures. This study emphasizes the significance of understanding fiber interactions in hybrid systems under cyclic loading, offering insights for future design and construction practices. As such, the findings are a valuable resource for engineers seeking to enhance performance and sustainability in practical applications. However, further research is necessary to fully understand the behavior of FR-SWSSC under varying load conditions. Additionally, long-term performance and durability in marine environments warrant further evaluation. Overall, the study underscores the promising potential of hybrid fibers for creating more resilient SWSSC structures.

CRediT authorship contribution statement

Milad Bazli: Writing – review & editing, Supervision. **Allan Manalo:** Writing – review & editing, Supervision. **Xing Ma:** Writing – review & editing, Supervision. **Christopher W.K. Chow:** Writing – review & editing, Supervision. **Yan Zhuge:** Writing – review & editing, Supervision. **Amirhesam Mashayekhi:** Writing – original draft, Validation, Methodology, Investigation, Formal analysis, Data curation, Conceptualization. **Reza Hassanli:** Writing – review & editing, Supervision, Project administration, Methodology, Investigation, Conceptualization.

Declaration of Competing Interest

The authors declare that they have no known competing financial interests or personal relationships that could have appeared to influence the work reported in this paper.

Data Availability

Data will be made available on request.

Acknowledgements

Financial support from the University of South Australia is gratefully acknowledged. The authors appreciate the technical expertise of the university's concrete laboratory technicians. We thank Adelaide Brighton Cement Ltd and Independent Cement and Lime Pty Ltd for donating OPC and GGBS, respectively, and TEXO company for their PPS and TPPL fiber donations, and the support of Mr. Adam Bromley. Acknowledgment is also extended to Dr. Murray Townsend and Mojtaba Karbasi from the Department for Environment and Water (DEW), as well as Spiros Dimas from the Department of Planning, Transport, and Infrastructure (DPTI), Government of South Australia, for their generous support in providing sea sand.Additionally, the valuable instrumentation and expertise of Microscopy Australia at the Future Industries Institute (FII), University of South Australia are acknowledged.

References

[1] S.A. Miller, A. Horvath, P.J. Monteiro, Impacts of booming concrete production on water resources worldwide, Nat. Sustain. 1 (1) (2018) 69–76.

[2] Y. Li, W. Liu, T. Mi, X. Ding, L. Tang, F. Xing, Durability study of seawater and sea-sand concrete under the combined effects of carbonation and chloride redistribution, J. Build. Eng. (2024) 109294.

[3] L. Zeng, X. Liang, H. Lu, S. Liu, H. Yuan, H.S. Mohamed, Compressive behavior of seawater and sea sand concrete-filled FRP-steel composite multi-tube hollow columns, Constr. Build. Mater. 438 (2024) 137133.

[4] P. Li, W. Li, Z. Sun, L. Shen, D. Sheng, Development of sustainable concrete incorporating seawater: A critical review on cement hydration, microstructure and mechanical strength, Cem. Concr. Compos. 121 (2021) 104100.

[5] M. Guo, B. Hu, F. Xing, X. Zhou, M. Sun, L. Sui, Y. Zhou, Characterization of the mechanical properties of eco-friendly concrete made with untreated sea sand and seawater based on statistical analysis, Constr. Build. Mater. 234 (2020) 117339.

[6] J. Xiao, C. Qiang, A. Nanni, K. Zhang, Use of sea-sand and seawater in concrete construction: Current status and future opportunities, Constr. Build. Mater. 155 (2017) 1101–1111.

[7] Slowey, K., *Report: Global construction waste will almost double by 2025.* Construction Dive, 2018.

[8] Y. Yu, G.-H. Fang, R. Kurda, A.R. Sabuj, X.-Y. Zhao, An agile, intelligent and scalable framework for mix design optimization of green concrete incorporating recycled aggregates from precast rejects, Case Stud. Constr. Mater. 20 (2024) e03156.

[9] Y. Yu, L. Zhou, L. Lin, Compressive stress–strain relationship and its variability of basalt fiber reinforced recycled aggregate concrete, AIP Adv. 14 (7) (2024).

[10] B. Lothenbach, K. Scrivener, R. Hooton, Supplementary cementitious materials, Cem. Concr. Res. 41 (12) (2011) 1244–1256.

[11] K.-H. Yang, Y.-B. Jung, M.-S. Cho, S.-H. Tae, Effect of supplementary cementitious materials on reduction of CO2 emissions from concrete, J. Clean. Prod. 103 (2015) 774–783.

[12] M.W. Tjaronge, U.R. Irfan, Porosity, pore size and compressive strength of self compacting concrete using sea water, Procedia Eng. 125 (2015) 832–837.

[13] X.-Q. CAO, Z.H.A.N.G. Y, H.E. Y.-J, J.I.A.N.G. Y.-C, Y.U.A.N. X.-J, Retrospect and discussion of surveys for construction sand in China offshore area, Mar. Geol. Quat. Geol. 28 (3) (2008) 121–125.

[14] T. Dhondy, A. Remennikov, M.N. Shiekh, Benefits of using sea sand and seawater in concrete: a comprehensive review, Aust. J. Struct. Eng. 20 (4) (2019) 280–289.

[15] Z. Xiong, S. He, A. Kwan, L. Li, Y. Zeng, Compressive behaviour of seawater sea-sand concrete containing glass fibres and expansive agents, Constr. Build. Mater. 292 (2021) 123309.

[16] D. Vafaei, R. Hassanli, X. Ma, J. Duan, Y. Zhuge, Sorptivity and mechanical properties of fiber-reinforced concrete made with seawater and dredged sea-sand, Constr. Build. Mater. 270 (2021) 121436.

[17] M. Etxeberria, A. Gonzalez-Corominas, P. Pardo, Influence of seawater and blast furnace cement employment on recycled aggregate concretes' properties, Constr. Build. Mater. 115 (2016) 496–505.

[18] M. Etxeberria, J.M. Fernandez, J. Limeira, Secondary aggregates and seawater employment for sustainable concrete dyke blocks production: Case study, Constr. Build. Mater. 113 (2016) 586–595.

[19] M.Z.Y. Ting, K.S. Wong, M.E. Rahman, M. Selowara Joo, Mechanical and durability performance of marine sand and seawater concrete incorporating silicomanganese slag as coarse aggregate, Constr. Build. Mater. 254 (2020) 119195.

[20] K. Katano, N. Takeda, Y. Ishizeki, K. Iriya, Properties and application of concrete made with sea water and un-washed sea sand, *Proc. Third Int. Conf. Sustain. Constr. Mater. Technol.* (2013).

[21] A. Younis, U. Ebead, P. Suraneni, A. Nanni, Fresh and hardened properties of seawater-mixed concrete, Constr. Build. Mater. 190 (2018) 276–286.

[22] D. Vafaei, X. Ma, R. Hassanli, J. Duan, Y. Zhuge, Microstructural behaviour and shrinkage properties of high-strength fiber-reinforced seawater sea-sand concrete, Constr. Build. Mater. 320 (2022) 126222.

[23] J. Ahmad, R.A. González-Lezcano, A. Majdi, N. Ben Kahla, A.F. Deifalla, M.A. El-Shorbagy, Glass fibers reinforced concrete: Overview on mechanical, durability and microstructure analysis, Materials 15 (15) (2022) 5111.

[24] Y. Li, J. Zhang, Y. He, G. Huang, J. Li, Z. Niu, B. Gao, A review on durability of basalt fiber reinforced concrete, Compos. Sci. Technol. 225 (2022) 109519.

[25] A. Mashayekhi, R. Hassanli, Y. Zhuge, X. Ma, C.W. Chow, Synergistic effects of fiber hybridization on the mechanical performance of seawater sea-sand concrete, Constr. Build. Mater. 416 (2024) 135087.

[26] J. Kaidi, W. Xin, D. Lining, C. Zhiyuan, H. Huang, L. Xia, L. Jianxun, W. Zhishen, Mechanical properties of multi-scale mono/hybrid non-metallic fiber-reinforced ultra-high performance seawater sea-sand concrete, Constr. Build. Mater. 401 (2023) 132922.

[27] D. Vafaei, R. Hassanli, X. Ma, J. Duan, Y. Zhuge, Fracture Toughness and Impact Resistance of Fiber-Reinforced Seawater Sea-Sand Concrete, J. Mater. Civ. Eng. 34 (5) (2022) 04022038.

[28] J. Feng, Y. Su, C. Qian, Coupled effect of PP fiber, PVA fiber and bacteria on self-healing efficiency of early-age cracks in concrete, Constr. Build. Mater. 228 (2019) 116810.

[29] Y. Ling, P. Zhang, J. Wang, Y. Chen, Effect of PVA fiber on mechanical properties of cementitious composite with and without nano-SiO2, Constr. Build. Mater. 229 (2019) 117068.

[30] Z. Zheng, and D. Feldman, *Synthetic fibre-reinforced concrete.* Prog. Polym. Sci. 20 (2) (1995) 185–210.

[31] R. Rostami, M. Zarrebini, M. Mandegari, D. Mostofinejad, S.M. Abtahi, A review on performance of polyester fibers in alkaline and cementitious composites environments, Constr. Build. Mater. 241 (2020) 117998.

[32] J.-P. Won, C.-I. Jang, S.-W. Lee, S.-J. Lee, H.-Y. Kim, Long-term performance of recycled PET fibre-reinforced cement composites, Constr. Build. Mater. 24 (5) (2010) 660–665.

[33] A.M. Alani, D. Beckett, Mechanical properties of a large scale synthetic fibre reinforced concrete ground slab, Constr. Build. Mater. 41 (2013) 335–344.

[34] A. Mashayekhi, R. Hassanli, Y. Zhuge, X. Ma, C.W. Chow, M. Bazli, A. Manalo, Synergistic effects of fiber hybridization on the fracture toughness of seawater sea-sand concrete, Constr. Build. Mater. 444 (2024) 137845.
[35] Z. Çelik, A.F. Bingöl, Fracture properties and impact resistance of self-compacting fiber reinforced concrete (SCFRC), Mater. Struct. 53 (3) (2020) 1–16.
[36] H. Pakravan, M. Jamshidi, M. Latifi, The effect of hydrophilic (polyvinyl alcohol) fiber content on the flexural behavior of engineered cementitious composites (ECC), J. Text. Inst. 109 (1) (2018) 79–84.
[37] J. Ríos, H. Cifuentes, C. Leiva, M. Ariza, M. Ortiz, Effect of polypropylene fibers on the fracture behavior of heated ultra-high performance concrete, Int. J. Fract. 223 (1) (2020) 173–187.
[38] S.F.U. Ahmed, H. Mihashi, Strain hardening behavior of lightweight hybrid polyvinyl alcohol (PVA) fiber reinforced cement composites, Mater. Struct. 44 (6) (2011) 1179–1191.
[39] Ö. Şükrü, Ç. Ömer, The hybrid effects of basalt and PVA fiber on properties of a cementitious composite: Physical properties and non-destructive tests, Constr. Build. Mater. 312 (2021) 125292.
[40] D.-L. Nguyen, D.-K. Thai, M.N.-T. Lam, Synergy in Flexure of High-Performance Fiber-Reinforced Concrete with Hybrid Steel Fibers, J. Mater. Civ. Eng. 34 (6) (2022) 04022090.
[41] K. Mehran, C. Mingli, X. Chaopeng, A. Majid, Effectiveness of hybrid steel-basalt fiber reinforced concrete under compression, Case Stud. Constr. Mater. 16 (2022) e00941.
[42] Y.M. Abbas, L.A. Hussain, M.I. Khan, Constitutive compressive stress–strain behavior of hybrid steel-PVA high-performance fiber-reinforced concrete, J. Mater. Civ. Eng. 34 (1) (2022) 04021401.
[43] C. Kai, X. Lihua, T. Tao, H. Le, L. Jian, H. Jian, L. Huan, C. Yin, Mechanical behavior of multiscale hybrid fiber reinforced recycled aggregate concrete subject to uniaxial compression, J. Build. Eng. 71 (2023) 106504.
[44] A.H. Abdel-Karim, G.I. Khalil, A.E. Ewis, M.H. Makhlouf, Impact of developed hybrid polypropylene fiber inclusion on the flexural performance of concrete beams reinforced with innovative hybrid bars, Constr. Build. Mater. 409 (2023) 134113.
[45] Z. Chenggong, W. Zhiyuan, Z. Zhenyu, G. Qiuyu, W. Xinrui, Z. Renda, Research on different types of fiber reinforced concrete in recent years: An overview, Constr. Build. Mater. 365 (2023) 130075.
[46] J. Ma, H. Yuan, J. Zhang, P. Zhang, Enhancing concrete performance: A comprehensive review of hybrid fiber reinforced concrete, *Structures* (2024).
[47] L. Gu, Y. Liu, J. Zeng, Z. Zhang, P.N. Pham, C. Liu, Y. Zhuge, The synergistic effects of fibres on mechanical properties of recycled aggregate concrete: A comprehensive review, Constr. Build. Mater. 436 (2024) 137011.
[48] V.S. Vairagade, S.A. Dhale, Hybrid fibre reinforced concrete–a state of the art review, Hybrid. Adv. 3 (2023) 100035.
[49] F. Deng, X. Ding, Y. Chi, L. Xu, L. Wang, The pull-out behavior of straight and hooked-end steel fiber from hybrid fiber reinforced cementitious composite: Experimental study and analytical modelling, Compos. Struct. 206 (2018) 693–712.
[50] M. Hsie, C. Tu, P. Song, Mechanical properties of polypropylene hybrid fiber-reinforced concrete, Mater. Sci. Eng.: A 494 (1-2) (2008) 153–157.
[51] D. Wang, Y. Ju, H. Shen, L. Xu, Mechanical properties of high performance concrete reinforced with basalt fiber and polypropylene fiber, Constr. Build. Mater. 197 (2019) 464–473.
[52] X. Du, Y. Li, Z. Si, L. Huang, X. Chen, Effects of basalt fiber and polyvinyl alcohol fiber on the properties of recycled aggregate concrete and optimization of fiber contents, Constr. Build. Mater. 340 (2022) 127646.
[53] W. Ahmed, C. Lim, Multicriteria performance assessment of sustainable recycled concrete produced via hybrid usage of basalt, polypropylene and glass fiber, Constr. Build. Mater. 397 (2023) 132462.
[54] Mashayekhi, A., R. Hassanli, Y. Zhuge, X. Ma, C.W. Chow, M. Bazli, and A. Manalo, *Synergistic Effects of Fiber Hybridization on the Fracture Toughness of Seawater Sea-Sand Concrete.* Construction and Building Materials, 2024.
[55] R. Oyguc, C. Toros, A.E. Abdelnaby, Seismic behavior of irregular reinforced-concrete structures under multiple earthquake excitations, Soil Dyn. Earthq. Eng. 104 (2018) 15–32.
[56] B. Boulekbache, M. Hamrat, M. Chemrouk, S. Amziane, Flexural behaviour of steel fibre-reinforced concrete under cyclic loading, Constr. Build. Mater. 126 (2016) 253–262.
[57] R. Park, T. Paulay, Reinforced concrete structures, John Wiley & Sons, 1991.
[58] J. Feng, X. Jia, X. Dong, P. Wang, B. Xu, Z. Wang, Cyclic compressive behavior of hook-end steel and macro-polypropylene hybrid fiber reinforced recycled aggregate concrete, Case Stud. Constr. Mater. 19 (2023) e02310.
[59] S. Wang, L. Xu, Y. Chi, K. Cui, C. Yin, B. Li, Cyclic tensile behavior of ultra-high performance concrete with hybrid steel-polypropylene fiber: Experimental study and analytical model, Compos. Struct. 321 (2023) 117255.
[60] K. Meng, L. Xu, Y. Chi, Experimental investigation on the mechanical behavior of hybrid steel-polypropylene fiber reinforced concrete under conventional triaxial cyclic compression, Constr. Build. Mater. 291 (2021) 123262.
[61] C. Wang, H. Wu, C. Li, Hysteresis and damping properties of steel and polypropylene fiber reinforced recycled aggregate concrete under uniaxial low-cycle loadings, Constr. Build. Mater. 319 (2022) 126191.
[62] H. Wu, Z. Zhu, Y. Chen, H. Li, W. Jiang, Mechanical properties of short polypropylene fiber enhanced recycled concrete under cyclic compression, Struct. Concr. 24 (4) (2023) 4751–4766.
[63] M.M. Sherif, E.M. Khakimova, J. Tanks, O.E. Ozbulut, Cyclic flexural behavior of hybrid SMA/steel fiber reinforced concrete analyzed by optical and acoustic techniques, Compos. Struct. 201 (2018) 248–260.
[64] M. De Smedt, R. Vrijdaghs, C. Van Steen, E. Verstrynge, L. Vandewalle, Damage analysis in steel fibre reinforced concrete under monotonic and cyclic bending by means of acoustic emission monitoring, Cem. Concr. Compos. 114 (2020) 103765.
[65] V.M. de Alencar Monteiro, L.R. Lima, F. de Andrade Silva, On the mechanical behavior of polypropylene, steel and hybrid fiber reinforced self-consolidating concrete, Constr. Build. Mater. 188 (2018) 280–291.
[66] R. de Souza Castoldi, L.M.S. de Souza, F. de Andrade Silva, Comparative study on the mechanical behavior and durability of polypropylene and sisal fiber reinforced concretes, Constr. Build. Mater. 211 (2019) 617–628.
[67] S. Yang, C. Zang, J. Xu, G. Fan, Determination of Fracture Parameters of Seawater Sea Sand Concrete Based on Maximum Fracture Load, J. Mater. Civ. Eng. 32 (1) (2020) 04019315.
[68] K.P. Fattah, A.K. Al-Tamimi, W. Hamweyah, F. Iqbal, Evaluation of sustainable concrete produced with desalinated reject brine, Int. J. Sustain. Built Environ. 6 (1) (2017) 183–190.
[69] Z.H. Zhang, Z.Q. Sang, L.Y. Zhang, Z.X. Ma, Y. Zhang, Experimental research on durability of concrete made by seawater and sea-sand, *Adv. Mater. Res.* (2013).
[70] C. Decision, Council Decision 2003/33/EC of 19 December 2002 establishing criteria and procedures for the acceptance of waste at landfills pursuant to Article 16 and Annex II to Directive 1999/31/EC, Off. J. Eur. Communities 16 (2003) (2003) 27–49.
[71] Australia, S., *Methods of testing concrete-Method 11: Determination of the modulus of rupture (AS 1012.11).* Sydney, NSW: Standards Australia, 2000.
[72] Australia, S., *Methods of testing concrete-Preparation of concrete mixes in the laboratory.* 1994, AS.
[73] F. Xie, D. Cai, L. Ji, C. Zhang, J. Ruan, Experimental study on the mechanical properties of internally cured concrete with super absorbent polymer under monotonic and cyclic loads, Constr. Build. Mater. 270 (2021) 121495.
[74] J. Wang, E. Liu, L. Li, Multiscale investigations on hydration mechanisms in seawater OPC paste, Constr. Build. Mater. 191 (2018) 891–903.
[75] Z. Yang, X. Zhan, H. Zhu, B. Zhang, P. Feng, H. Li, H.W. Kua, Performance-based alkali-activated seawater sea-sand concrete: Mixture optimization for mechanical, environmental, and economical objectives, Constr. Build. Mater. 409 (2023) 134156.
[76] M. Li, D. Xing, Q.-B. Zheng, H. Li, B. Hao, P.-C. Ma, Variation on the morphology and tensile strength of basalt fiber processed in alkali solutions, Constr. Build. Mater. 335 (2022) 127512.
[77] Q. Wang, Y. Ding, N. Randl, Investigation on the alkali resistance of basalt fiber and its textile in different alkaline environments, Constr. Build. Mater. 272 (2021) 121670.
[78] R. Hassanli, A. Manalo, D. Vafaei, M. Yekrangnia, M. Elchalakani, M. Noël, Cyclic behavior of GFRP-reinforced concrete one-way slabs with synthetic fibers, J. Build. Eng. 65 (2023) 105741.
[79] A. Shoaib, A.S. Lubell, Effect of mix composition on the mechanical properties of SFRC, Constr. Build. Mater. 286 (2021) 122760.
[80] A.K.F. Gaddafi, U.J. Alengaram, N.M. Bunnori, S.I. Muhammad, S. Ibrahim, M. Sumesh, Mechanical properties, flexural behaviour, and ductility characteristics of fibre-reinforced geopolymer mortar, Constr. Build. Mater. 403 (2023) 133109.
[81] J.-H. Lee, B. Cho, E. Choi, Flexural capacity of fiber reinforced concrete with a consideration of concrete strength and fiber content, Constr. Build. Mater. 138 (2017) 222–231.
[82] Society, C., Concrete industrial ground floors: A guide to design and construction. 2003: Concrete Society.
[83] SF, J., *Method of test for flexural strength and flexural toughness of fiber reinforced concrete.* Japan Concrete Institute, 1984.
[84] J. Wei, N. Farzadnia, K.H. Khayat, Synergistic effect of macro synthetic fiber and shrinkage-reducing admixture on engineering properties of fiber-reinforced super-workable concrete, Constr. Build. Mater. 414 (2024) 134566.
[85] J.-H. Lee, K.-J. Lee, E. Choi, Flexural capacity and crack-closing performance of NiTi and NiTiNb shape-memory alloy fibers randomly distributed in mortar beams, Compos. Part B: Eng. 153 (2018) 264–276.
[86] J.-H. Lee, B. Cho, J.-B. Kim, K.-J. Lee, C.-Y. Jung, Shear capacity of cast-in headed anchors in steel fiber-reinforced concrete, Eng. Struct. 171 (2018) 421–432.
[87] Astm, C., 1609. Standard test method for flexural performance of fiber-reinforced concrete (using beam with third-point loading), 2007. 4.
[88] Ş. Özkan, F. Demir, The hybrid effects of PVA fiber and basalt fiber on mechanical performance of cost effective hybrid cementitious composites, Constr. Build. Mater. 263 (2020) 120564.
[89] W.-l Min, W.-l Jin, X.-y He, R.-j Wu, K.-y Chen, J.-j Chen, J. Xia, Experimental study on the flexural fatigue performance of slag/fly ash geopolymer concrete reinforced with modified basalt and PVA hybrid fibers, J. Build. Eng. (2024) 109917.